Precipitation of Carbonate Minerals Induced by the Halophilic *Chromohalobacter Israelensis* under High Salt Concentrations: Implications for Natural Environments

Zuozhen Han [1,2,*,†], Dan Li [1,†], Hui Zhao [2,3,†], Huaxiao Yan [2,3,*] and Peiyuan Li [1]

[1] Shandong Provincial Key Laboratory of Depositional Mineralization and Sedimentary Minerals, College of Earth Science and Engineering, Qingdao 266590, China; ldlxy1990@163.com (D.L.); m17854253816@163.com (P.L.)

[2] Key Laboratory of Marine Geology and Environment, Chinese Academy of Sciences, Qingdao 266071, China; zhsdust@126.com

[3] Department of Bioengineering, College of Chemical and Environmental Engineering, Shandong University of Science and Technology, Qingdao 266590, China

* Correspondence: hanzuozhen65@126.com (Z.H.); 15954804511@163.com (H.Y.)

† These authors contributed equally to this work.

Abstract: The precipitation of carbonate minerals induced by halophilic bacteria has aroused wide concern. The study aimed to investigate the characterization and process of biomineralization in high salt systems by halophilic *Chromohalobacter israelensis* LD532 (GenBank: KX766026) bacteria, isolated from the Yinjiashan Saltern in China. Carbonate minerals were induced in magnesium sulfate and magnesium chloride medium, respectively. The mineral phase, morphology, and elemental composition of minerals were analyzed using X-ray p owder diffraction, scanning electron microscopy, and energy dispersive X-ray detection. Cells and ultrathin slices were studied using high resolution transmission electron microscopy, selected area electron diffraction, and energy dispersive X-ray detection. The carbonic anhydrase and ammonia released from LD532 bacteria increased pH of the medium and promoted the carbonate precipitation. Magnesium calcite and aragonite were induced by LD532 bacteria in magnesium chloride medium at an Mg/Ca molar ratio of 2, while Magnesium calcite and monohydrocalcite were precipitated in magnesium sulfate medium at the same Mg/Ca ratio, only monohydrocalcite were formed in both control groups. The morphologies and compositions of minerals in $MgSO_4$ and $MgCl_2$ solutions displayed significant differences, indicating different Mg^{2+} could affect physiological and biochemical activities of LD532 bacteria and thus affect the mineral deposition. Further study showed the nucleation sites were located on extracellular polymeric substances and intracellular vesicles of LD532 bacteria. This study is beneficial to the mechanism of carbonate biomineralization in natural salt environments.

Keywords: biomineralization; halophilic bacteria; magnesium chloride; magnesium sulfate; Mg/Ca ratios; nucleation sites

1. Introduction

Carbonate minerals are widely distributed in the Earth's crust and play an important role in the study of early diagenesis of marine sediments, calcification and the formation of cavernous chemical deposits [1]. In recent decades, many cyanobacterial fossils have been discovered in biolith, which confirms that microbes are closely associated with the diagenesis of minerals. Based on previous

research findings on bioliths, such as stromatolites, oncolites, dendrites, and thrombolites [2–10], many researchers have investigated the ability of bacteria to precipitate minerals in natural environments and the laboratory. Therefore, the role of microorganisms in the precipitation of a wide variety of carbonates generally has been acknowledged in recent years [11]. Interactions between microorganisms and minerals are a type of geological activities that occur widely in natural environments, and mineral dissolution and precipitation are almost inseparable from the role of microorganisms. Microbial mineralization can be traced back to the more distant geological past. For example, the development of large-scale stromatolites and iron-rich formations occurred during the Precambrian. Therefore, carbonate precipitation induced by different species of bacteria was a very common event in natural environments [5]. The changes of aragonite saturation in seawater induced by the bloom-forming filamentous diazotroph *Trichodesmium* at different levels of phosphorus (P) availability have been described [12]. The morphology and mineralogy of carbonate minerals can be influenced by sulfate-reducing bacteria, which can produce copious amounts of extracellular polymeric substances (EPS) and increase the alkalinity by sulfate reduction and consumption of organic acids [13,14]. Many researchers have studied the formation of calcite crystals on EPS secreted by *Bacillus firmus*, *Bacillus sphaericu*, and *Synechocystis* sp. *PCC6803* [15–17].

In addition, the precipitation mechanisms of minerals have not been uniformly recognized, while many scholars have studied the process of biomineralization. Some researchers have argued that bacteria can induce the formation of different types of carbonates under appropriate conditions [18]. The biomineralization of carbonates and other types of minerals is caused by the participation of specific macromolecules originating from bacteria in the culture medium [19]. The activities of urease and carbonic anhydrase (CA) play an important role in microbiologically induced carbonate precipitation [20]. The biomineralization mechanism of *Bacillus* has also been studied in the process of carbonate precipitation [21]. However, controversies still exist regarding the specific role that different bacteria play in the formation process of microbial carbonates in many cases [2,22,23], for example, the similarity of spherulitic and dumbbell-shaped growth process of carbonate minerals induced by different microorganism still needs to be investigated [17,24], the difference between elemental composition of the mineral formed by bio-mineralization method and physical chemistry method also needs to be studied [25], as well as the role of organic functional groups playing on the nucleation and growth of minerals should also be explored [26].

Researchers have suggested that the composition and ionic concentration of the solution exert a considerable influence on the mineral precipitation in geological environments, and have also shown that acicular high-Mg calcite or aragonite can be produced in seawater with a high Mg/Ca ratio or in high-salinity lakes [27]. The element Mg is involved in almost all of the geochemical processes relative to the formation of carbonate rocks, especially dolomite [28]. Calcite mineralization can be controlled by the Mg/Ca ratio of seawater [29]. Ca, Mg and Mg/Ca ratios have an effect on the precipitation of Mg-rich carbonates [30]. The concentration of Mg^{2+} has some influence on the structure of monohydrocalcite during its formation process [31].

In recent years, the precipitation of carbonates induced by halophilic bacteria has been an important topic. Moderately halophilic bacteria are those that grow optimally at 3–15% (*w/v*) NaCl. Halophiles can survive under high-salt conditions because of their special cellular structure and metabolic mechanism. In previous studies, several researchers have observed different minerals induced by halophilic bacteria under different conditions. A moderately halophilic bacterium, *Chromohalobacter marismortui*, which was isolated from the Dead Sea by Elazari Volcani in 1940, has been described [32], and the precipitation of minerals by microorganisms was studied for the first time using *Chromohalobacter marismortui* [7]. The carbonate precipitation induced by *Halomonas mónica* has been studied under different salt concentrations and incubation conditions, and the mineral phases produced were analyzed [5,33]. The mechanism of mineralization induced by halophilic bacteria has also been studied by a number of researchers. The cellular envelopes of bacteria provided nucleation sites in the process of carbonate precipitation [5–8,10,30]. The EPS and the cell walls were identified as

the nucleation sites [34]. Based on the studies mentioned above, it can be seen that the mechanism of microbiologically induced carbonate precipitation has not been thoroughly characterized, although numerous scholars and experts have specifically investigated questions regarding minerals induced by bacteria. For example, what an important role of halophilic bacteria played in the surface morphology, mineral phase and elemental composition of carbonate minerals at different Mg/Ca ratios, different sources of Mg ions, and high concentrations of NaCl. Therefore, the mechanism of biomineralization still requires in-depth exploration.

In this paper, the precipitation of carbonate induced by *Chromohalobacter israelensis* LD532 bacterium, which was isolated from the Yinjiashan Saltern in China, was studied under experimental conditions, including high-salt (NaCl) concentrations, varying Mg/Ca ratios (0, 2, 4, 6, 8, and 10), and different Mg^{2+} sources. The experimental groups were inoculated with 1% of *C. israelensis* LD532 bacterial liquid seed, and the control groups were inoculated with the same volume of sterile distilled water. X-ray diffraction (XRD), scanning electron microscopy (SEM), and energy dispersive X-ray detection (EDS) were used to study the mineralogy and morphology of the carbonate crystals induced by *C. israelensis* LD532 bacteria. The organic functional groups originating from LD532 bacteria in carbonate minerals were analyzed using Fourier transform infrared spectroscopy (FTIR). High-resolution transmission electron microscopy (HRTEM), selected area electron diffraction (SAED), and energy dispersive spectrometry (EDS) were used to analyze the morphology and elemental composition of mineral crystals located on the EPS of *C. israelensis* LD532 bacteria. To further determine the nucleation sites of carbonate minerals, ultra-thin slices of *C. israelensis* LD532 bacteria in $MgSO_4$ and $MgCl_2$ culture media were prepared and observed using transmission electron microscopy (TEM), SAED, and EDS. CA was also investigated in order to further explore the mechanism of microbially induced carbonate minerals. The study provides a reference for interpretation the formation mechanism of carbonate minerals in the geological record, is beneficial to understanding microbial mineralization in natural and laboratory environments, and also helps to explain the origins of ancient carbonate sedimentary environments.

2. Materials and Methods

2.1. Culture Medium

A liquid culture medium was used for the enrichment of halophilic bacteria with the following composition (g L^{-1}): beef extract 5.0, tryptone 10.0, and NaCl 150. The pH of the culture medium was 7.2. Twenty grams of agar powder was added into the above liquid medium to form the solid medium. The above culture medium was used to isolate and purify the halophilic bacteria.

2.2. Isolation, Identification and Micromorphology of C. israelensis LD532 Bacterium

LD532 bacteria were isolated from water samples collected from the Yinjiashan Saltern (35°48′ N, 119°55′ E) in Qingdao, China. The water sample was added into the liquid enrichment culture medium (inoculation volume: 1%, *v/v*), and incubated in a constant temperature shaker (HZQ-F160, Harbin Donglian Electronic Technology Development Co., Ltd., Harbin, China) at 130 rpm and 30 °C. The medium turned turbid after 2 days of culture, indicating that several dominant types of halophilic bacteria were present. The change in transparency was mainly attributable to the physiological and biochemical activities of halophilic bacteria. The turbid enrichment medium was diluted 100-fold using sterile distilled water, and the diluent was spread evenly over the surface of the solid medium for further isolation and purification. All of the bacterial cultures were incubated in an electrothermal constant temperature incubator (DHP-9050B, Shanghai Langgan Laboratory Equipment Co., Ltd., Shanghai, China) at 30 °C until single colonies could be seen by the naked eye. A single bacterial colony was then selected and purified 3 times. A pure strain named LD532 was obtained and identified by physiological and biochemical identification and 16S rDNA identification [35].

Bacterial genomic DNA was extracted with the improved cetyltrimethylammonium bromide (CTAB) method [36] and used as a template for PCR. The 16S rDNA gene sequences were amplified with universal primers 27F (5′-agagtttgatcatggctcag-3′) and 1492R (5′-tacggttaccttgttacgactt-3′) [37]. The PCR products were then analyzed via agarose gel electrophoresis. Gene fragments in agarose gel approximately 1500 bp long were the expected products. The PCR products were sequenced by Shanghai Sangon Biotech Co., Ltd. (Shanghai, China). The complete DNA sequence was obtained through fragment assembly using DNAMAN 8.0 software. Subsequently, a nucleotide homology comparison was carried out using the Basic Local Alignment Search Tool (BLAST) software package (NLM, Bethesda, MD, USA). The phylogenetic tree of LD532 was constructed using MEGA 5.0 software with a neighbor-joining method [38]. The 16S rDNA sequence of *C. israelensis* LD532 has been deposited in GenBank under accession number KX766026.

The micromorphology of *C. israelensis* LD532 bacterium was observed. After 10 days of incubation at 30 °C, a single colony on the surface of the solid medium, with a diameter of approximately 5 mm, was transferred to a 1.5-mL centrifuge tube and diluted with 200 μL of sterile distilled water. The above diluent was dripped onto a copper grid before being analyzed by TEM (JEM-2100, Japan Electronics Company, JEOL, Tokyo, Japan) after natural drying.

2.3. Growth of C. israelensis LD532 Bacteria at Different NaCl Concentrations and pH Values

The growth curve of LD532 bacteria in the liquid culture medium was described. The composition of the liquid medium was as follows (g L^{-1}): beef extract 5.0, tryptone 10.0, and NaCl 100.0. The pH of the liquid medium was 7.2. Three parallel samples have been set in each group. Cell concentrations were positively correlated with OD values. The cell concentration can be calculated according to the equation that the OD values multiply 0.8×10^9. Therefore, the OD value can be used to obtain cell growth through the relationship between OD value and cell concentration. The OD value of LD532 bacteria was measured using a spectrophotometer (722 s, Shanghai Precision and Scientific Instrument Corporation, Shanghai, China) at 600 nm. At the same time, the fermentation liquid was used as liquid seed when the value measured with the spectrophotometer at 600 nm was approximately 0.9.

The growth of LD532 bacteria under different salt (NaCl) concentrations was studied. The concentrations of NaCl were 3, 5, 8, 10, 12, 15, 18, and 20% (*w/v*). Three parallel samples have been set in each group. The above liquid seed was inoculated into the liquid culture medium with different concentrations of NaCl and cultivated under the following conditions: inoculation volume 1% (*v/v*), rotate speed 130 rpm, and temperature 30 °C. After 24 h, the concentration of LD532 bacteria was measured with the spectrophotometer at 600 nm.

The growth of LD532 bacteria under different pH conditions was also studied. The pH value of the above liquid medium was adjusted to 5.0, 5.5, 6.0, 6.5, 7.0, 7.5, 8.0, 8.5, 9.0, and 9.5. Three parallel samples have been set in each group. The concentration of LD532 bacteria was measured with the spectrophotometer at 600 nm after 24 h.

2.4. Growth and pH Curves of LD532 Bacteria at Different Mg/Ca Molar Ratios

The growth and pH curves of LD532 bacteria at different Mg/Ca ratios were studied. The concentration of Ca^{2+} stock solution was 0.01 M. MgSO$_4$ (2 M), MgCl$_2$ (2 M), Na$_2$CO$_3$ (2 M), and NaHCO$_3$ (1 M) mother liquors were prepared according to the conventional method. The composition of the liquid medium was as follows (g L^{-1}): beef extract 5.0, tryptone 10.0, NaCl 150.0. Three milliliters of Na$_2$CO$_3$ (2 M) and 6 mL of NaHCO$_3$ (1 M) were added into each conical flask containing 150 mL of the culture medium, and the pH was adjusted to 7.3. Mg/Ca molar ratios were 0, 2, 4, 6, 8, and 10, respectively, and three control groups and three experimental groups were respectively set in the group with same Mg/Ca molar ratio. All of the cultures were incubated in the constant temperature shaker at 130 rpm and 30 °C. The concentrations of LD532 bacteria were measured with the spectrophotometer at 600 nm at different time intervals. The pH values were measured using a pH indicator (PHS-3, Jiangsu Jiangfen Instrument and Equipment Company, Jiangsu, China) at different time intervals.

2.5. CA Activity of C. israelensis LD532 Bacteria in the Liquid Culture Medium

To understand the biomineralization mechanism of *C. israelensis* LD532 bacteria, the CA activity of *C. israelensis* LD532 bacteria was examined in the liquid culture medium with an Mg/Ca molar ratio of 2, 15% NaCl, and pH 7.2. CA activity was detected according to the method described by Smith and Ferry [39], and one unit of CA was defined as the amount of enzyme that released 1 μmol of *p*-nitrophenol per minute.

2.6. Characterization of Carbonates Induced by C. israelensis LD532 Bacteria

Precipitates in the control and experimental groups at different Mg/Ca molar ratios were transferred from the bottom of the flask to 4-mL centrifuge tubes, and let stand 10 min. To fully eliminate the bacteria, the deposits were washed 3 times with distilled water after the supernatant was discarded, then washed 3 times with anhydrous ethanol and dried in air at room temperature.

To identify the mineral phases of the carbonates induced by *C. israelensis* LD532 at different Mg/Ca ratios, the precipitates mentioned above were studied by XRD (D/Max-RC, Rigaku, Tokyo, Japan) using 2θ angles ranging from 10 to 75 °C, a step size of 0.02, and a count time of 8° min^{-1}. At the same time, to further determine whether organic functional groups existed in the carbonate minerals, the precipitates were also analyzed by FTIR (Nicolet 380, Thermo Fisher Scientific Inc., Waltham, MA, USA) using a scanning range of 4000–400·cm^{-1}.

The shapes, sizes, and micromorphologies of the precipitates were also observed. The mineral precipitates in the control and experimental groups were sprayed with platinum (Pt) in vacuum and observed with SEM (Hitachi S-4800, Hitachi, Tokyo, Japan) after they were dried naturally. The elemental composition of the mineral precipitates was analyzed using EDS (EDAX, Mahwah, NJ, USA).

2.7. Minerals on the Surfaces of C. israelensis LD532 Bacteria

To assess whether the EPS of *C. israelensis* LD532 bacteria was the nucleation site, *C. israelensis* LD532 bacterial suspension in the experimental group at an Mg/Ca molar ratio of 2 was dripped onto a copper grid and then observed with HRTEM (JEM-2100UHR, JEOL) after drying naturally. The crystalline structure and elemental composition of the precipitates on the EPS were analyzed with SAED (Gatan-832, Pleasanton, CA, USA) and EDS (EDAX, Mahwah, NJ, USA).

2.8. Analysis of Ultra-Thin Slices of C. israelensis LD532 Bacteria

The ultra-thin slices of *C. israelensis* LD532 bacterial cells, cultivated for 40 days, were prepared as follows: 10 mL of LD532 bacterial fermentation liquid at an Mg/Ca molar ratio of 2 was centrifuged at a speed of 3000 rpm for 5 min. The supernatant was discarded, and the deposit was washed 3 times with phosphate buffer (NaH$_2$PO$_4$·2H$_2$O: 3.1167 g/L, Na$_2$HPO$_4$·12H$_2$O: 20.7472 g/L, pH 7.4) to remove the remaining culture medium. *C. israelensis* LD532 cells were fixed with 1 mL of 2.5% glutaraldehyde and 1% osmic acid for 1 h, and washed 3 times with phosphate buffer. The cells were then dehydrated in different concentrations of acetone with the following sequence: 30% (15 min)–50% (15 min)–70% (15 min)–80% (15 min)–90% (15 min)–95% (15 min)–100% (15 min)–100% (15 min)–100% (15 min). One milliliter of 30% epoxy resin solution was then added, and the cells were embedded. The completed ultra-thin slices were analyzed with TEM (JEM-2011, JEOL).

3. Results

3.1. Identification of C. israelensis LD532 Bacteria

C. israelensis LD532 bacterium is a gram-negative, strictly aerobic, and rod-shaped bacterium with a width of approximately 0.5 to 0.8 μm and a length of approximately 0.7 to 1.5 μm (Table 1, Figure 1a,b). LD532 bacterium can move in the semisolid medium (Table 1), indicating that the bacteria

are motile. Bacteria commonly derive their motility from external structures called flagella. It can be seen from Figure 1a,b that more than one flagellum grows on the surface of LD532 bacterium, which also demonstrates its motility (Table 1). The results of physiological and biochemical identifications are shown in Table 1. Ammonia, amylase, citrate, EPS, motility, and urease tests are positive, while the V-P, catalase, sulfureted hydrogen, methyl red, cellulase, and esterase tests are negative. The result of TSI shows that LD532 bacteria can use lactose to produce a large amount of acid to make the medium yellow, no gas is produced, and the bottom of the tube does not turn black, indicating LD532 bacteria could not use sulfur-containing amino acids.

The 16S rDNA sequence of LD532 is 1452 bp, determined using DNAMAN 8.0 to join complementary sequences. A nucleotide homology comparison was conducted with the BLAST program. A phylogenetic tree was constructed with MEGA 5.0 software using the neighbor-joining method (Figure 2). The full-length 16S rDNA sequence of strain LD532 shares >97% nucleotide sequence homology with the 16S rDNA sequences of many *Chromohalobacter* strains in GenBank, and 98% homology with those of three strains of *C. israelensis*. The strain LD532 is most closely related to *C. israelensis* on the phylogenetic tree based on 16S rDNA sequences, which is consistent with the physiological and biochemical characteristics of the isolated strain. Thus, strain LD532 has been identified as *C. israelensis*.

Table 1. The physiological and biochemical identification of *C. israelensis*.

Test Item	LD532
Ammonia	+
V-P	−
Catalase	−
Sulfureted Hydrogen	−
Amylase	+
Methyl Red	−
Citrate	+
Cellulase	−
EPS	+
Moveability	+
Esterase	−
Urease	+
Triple Sugar Iron Agar	no gas brown yellow no black precipitates

Note: The "−" is negative; the "+" is positive.

(a)　　　　　　　　　　　(b)
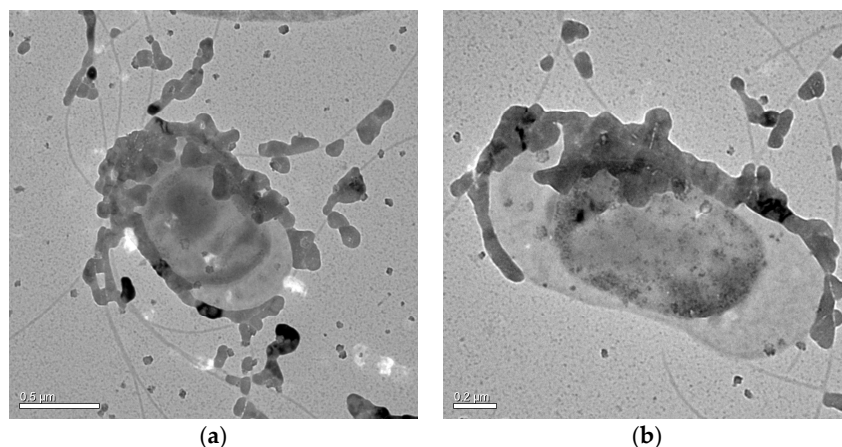
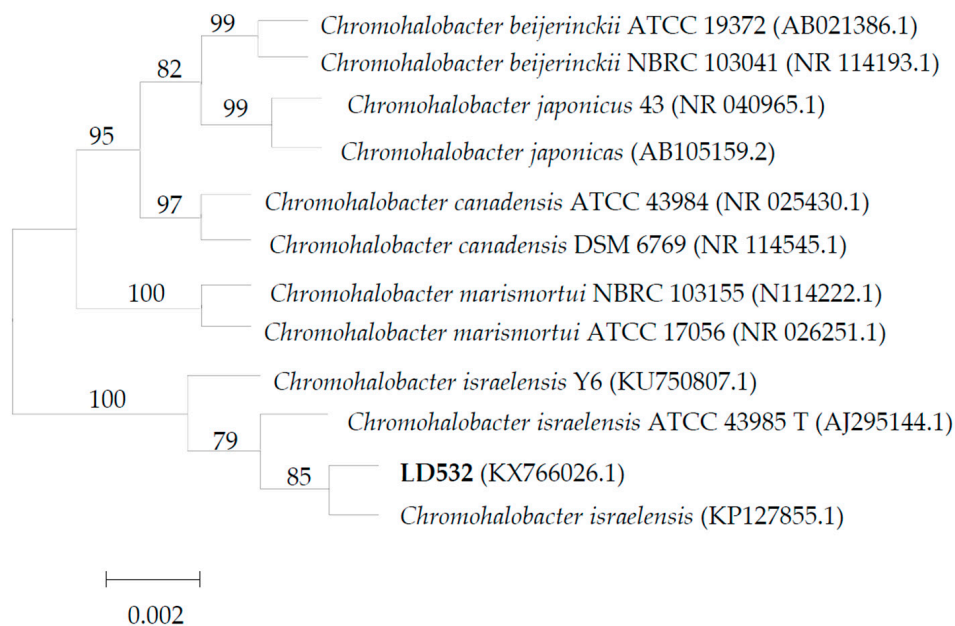**Figure 1.** The morphology of LD532 bacteria analyzed by HRTEM.

```
      99 ┌─ Chromohalobacter beijerinckii ATCC 19372 (AB021386.1)
   82 ┌──┤
      │  └─ Chromohalobacter beijerinckii NBRC 103041 (NR 114193.1)
      │  99 ┌─ Chromohalobacter japonicus 43 (NR 040965.1)
95 ┌──┤  ┌──┤
   │  └──┤  └─ Chromohalobacter japonicas (AB105159.2)
   │     97 ┌─ Chromohalobacter canadensis ATCC 43984 (NR 025430.1)
   │     ┌──┤
   │     │  └─ Chromohalobacter canadensis DSM 6769 (NR 114545.1)
   │  100 ┌─ Chromohalobacter marismortui NBRC 103155 (N114222.1)
   │  ┌───┤
   │  │   └─ Chromohalobacter marismortui ATCC 17056 (NR 026251.1)
100 ┌──── Chromohalobacter israelensis Y6 (KU750807.1)
 ┌──┤
 │  │  79 ┌─ Chromohalobacter israelensis ATCC 43985 T (AJ295144.1)
 │  └──┤
 │     │  85 ┌─ LD532 (KX766026.1)
 │     └──┤
 │        └─ Chromohalobacter israelensis (KP127855.1)
```

├──────┤
0.002

Figure 2. Phylogenetic tree of LD532 bacteria.

3.2. The Growth Curves of C. israelensis LD532 Bacteria in Liquid Culture Medium at Different Salt Concentrations and pH Values

Figure 3a shows the growth curve of bacterial strain LD532 incubated in the liquid culture medium with a NaCl concentration of 15% (*w*/*v*) at 30 °C for 120 h. It can be seen that the bacteria grow slowly during the initial 3 h, the cells are in the logarithmic growth stage between 3 and 45 h, and after 45 h, the bacterial growth declines. Figure 3b shows the growth curve of bacterial strain LD532 incubated in the liquid culture medium with different NaCl concentrations at 30 °C for 24 h, and the results indicate that the bacteria grew best at a NaCl concentration of 10% among the investigated NaCl concentrations ranging from 3% to 20%. Figure 3c shows the growth curve of bacterial strain LD532 incubated in the liquid culture medium with different pH values and a NaCl concentration of 15% at 30 °C for 24 h. The result shows that the bacteria grew normally under pH values ranging from 5.0 to 8.5, but the cell concentrations declined sharply when the pH was increased above 8.5, and the bacteria almost stopped growing at pH values of 9.0 and 9.5. According to the above results, culture conditions, such as the liquid culture medium, pH of 7.3, and a NaCl concentration of 15%, were appropriate for LD532 bacteria in the following experiments to investigate carbonate precipitation.

3.3. Growth, pH, and CA Activity Curves of LD532 Bacteria

Figure 4a shows the growth curves of LD532 bacteria at different Mg/Ca ratios and a NaCl concentration of 15%. It can be seen from Figure 4a that, at each Mg/Ca ratio (0, 2, 4, 6, 8, and 10), the bacteria grow slowly during the first 9 h, the cell concentrations increase sharply from 9 to 50 h in the logarithmic growth phase, and the bacteria are in a stable phase from 50 to 100 h. During this last phase, the cell concentrations of LD532 bacteria increase slightly with increasing Mg/Ca ratios. According to the above results, it can be seen that, within limits, the influence of Mg is quite weak on the growth of the bacteria in this experiment.
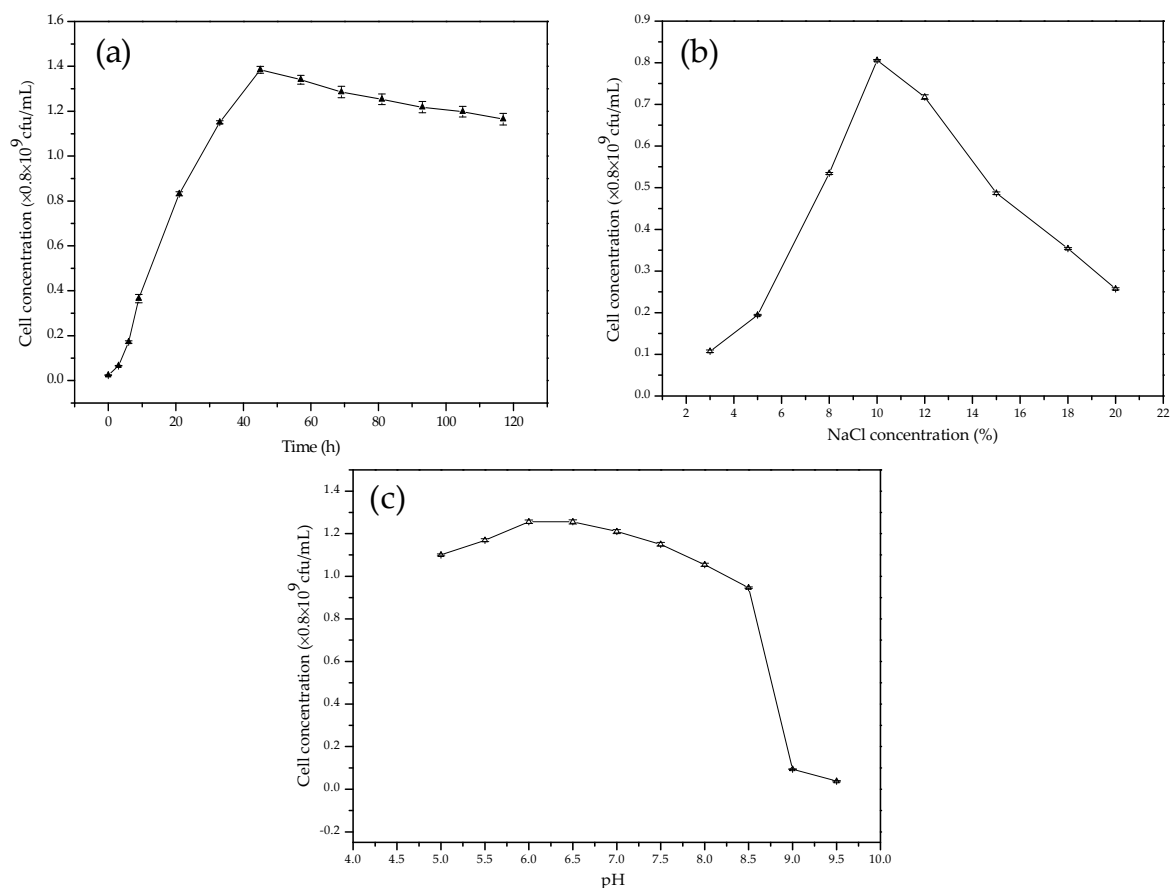
Figure 3. Characterization of LD532 bacteria: (**a**) growth curve; (**b**) cell concentration of LD532 bacteria after the 24 h cultivation at different NaCl concentrations; and (**c**) cell concentration of LD532 bacteria after the 24 h cultivation at different pH values.

To determine the mechanism responsible for the increasing pH values, the changes in CA activity were also investigated (Figure 4b). Comparison with Figure 4a shows that CA was a synchronous synthase because of the coupling of this enzyme with the growth of bacteria. At the beginning, the quantity of CA released is very small. The production of CA increases sharply from approximately 1 to 99 U·mL^{-1}, and accompanies a sharp increase of LD532 bacteria during the logarithmic phase. It decreases during the bacterial stable phase and reaches 26 U·mL^{-1} by the end of the experiment.

Figure 4c shows the pH curves of LD532 bacteria at different Mg/Ca ratios and a NaCl concentration of 15%. It can be seen from Figure 4c that the pH increases sharply, from 7.3 to 8.7, during the first 9 h, due to the release of ammonia from the liquid seed. It declines slowly, from 8.7 to 8.3, during 9–24 h, owing to the release of carbon dioxide produced by LD532 bacteria. A slight increase in pH from approximately 8.3 to 8.8 occurs during 24–60 h; in this period, the concentration of CA secreted by LD532 bacteria increases to 99 U·mL^{-1} from approximately 1 U·mL^{-1} (Figure 4b). The pH values decrease from approximately 8.8 to 8.4 during the period of 60–96 h, during which time the CA activity declines from 99 to 26 U·mL^{-1} (Figure 4b). Finally, the pH values increase slowly from approximately 8.5 to 9.0 (Figure 4c) in the time range of 96–168 h. It is more notable that the pH value increases to approximately 8.8 at an Mg/Ca ratio of 10. The values of pH are stable during the period of time from 168–220 h, approximately 9.0 at Mg/Ca ratios of 0, 2, 4, 6, and 8, and approximately 8.8 at an Mg/Ca ratio of 10. During the pH-stable phase, the pH values decrease with increasing Mg/Ca ratios, which is closely connected with the fact that, at higher Mg/Ca ratios, the higher cell concentrations of LD532 bacteria could produce greater amounts of carbon dioxide. According to the above results, the pH values could reach approximately 9.0, due to the CA and ammonia released from

C. israelensis LD532 bacteria, which was taken as a necessary condition for the biomineralization of bacterially induced carbonates.
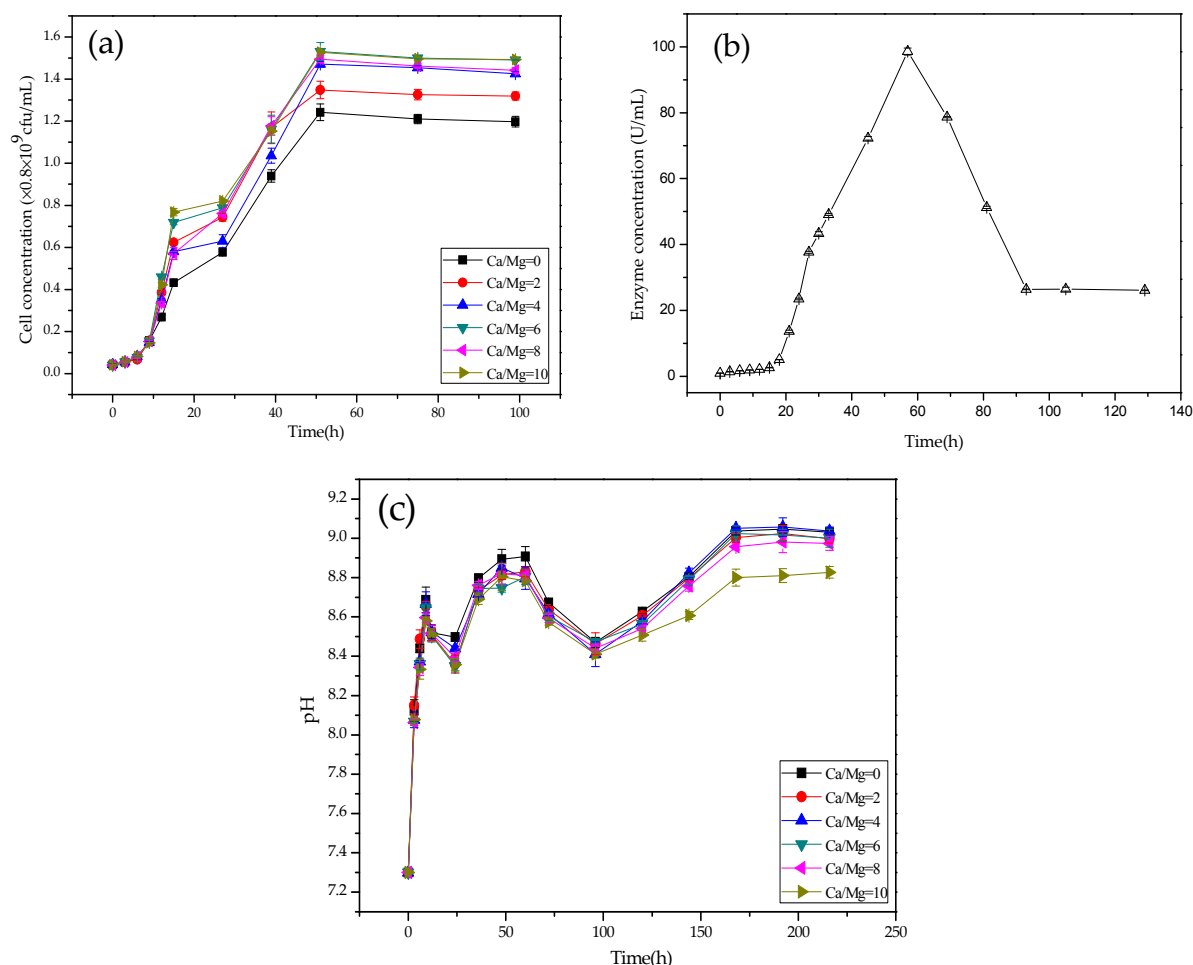

Figure 4. Growth curves, enzyme activity curve and pH curves of LD532 bacteria at different Mg/Ca molar ratios: (**a**) growth curves; (**b**) CA activity curve; and (**c**) pH curves.

3.4. Carbonate Minerals Analyzed by XRD and FTIR

To further analyze the mineral phases and structural characteristics of the precipitates induced by *C. israelensis* LD532 bacteria, the carbonate precipitates after 15 days of culture were analyzed using XRD. The results of the mineralogical analysis are displayed in Figures 5 and 6.

It can be seen from Figure 5 that the minerals in the control and experimental groups containing $MgSO_4$ are calcite at an Mg/Ca ratio of 0 (Figure 5a,b), and monohydrocalcite is the only precipitate in the control group at other Mg/Ca ratios (Figure 5a). In contrast, there is a significant difference in the mineral phases between the control group and the experimental group at an Mg/Ca ratio of 2; Mg-calcite, in addition to monohydrocalcite, formed in the experimental group (Figure 5b). The Mg contents of Mg-calcite were determined to be 27%, by applying the appropriate equation [40,41]. The minerals in the experimental group at other Mg/Ca ratios are the same as those in the control group. It is worth noting that, in the control group, the diffraction peak intensity associated with the (222) crystal plane is higher than that of the (411) crystal plane at Mg/Ca ratios of 4 and 6 (Figure 5a), which contrasts with the standard diffraction peak intensity of monohydrocalcite, indicating that monohydrocalcite with a preferred orientation was precipitated in this experiment.
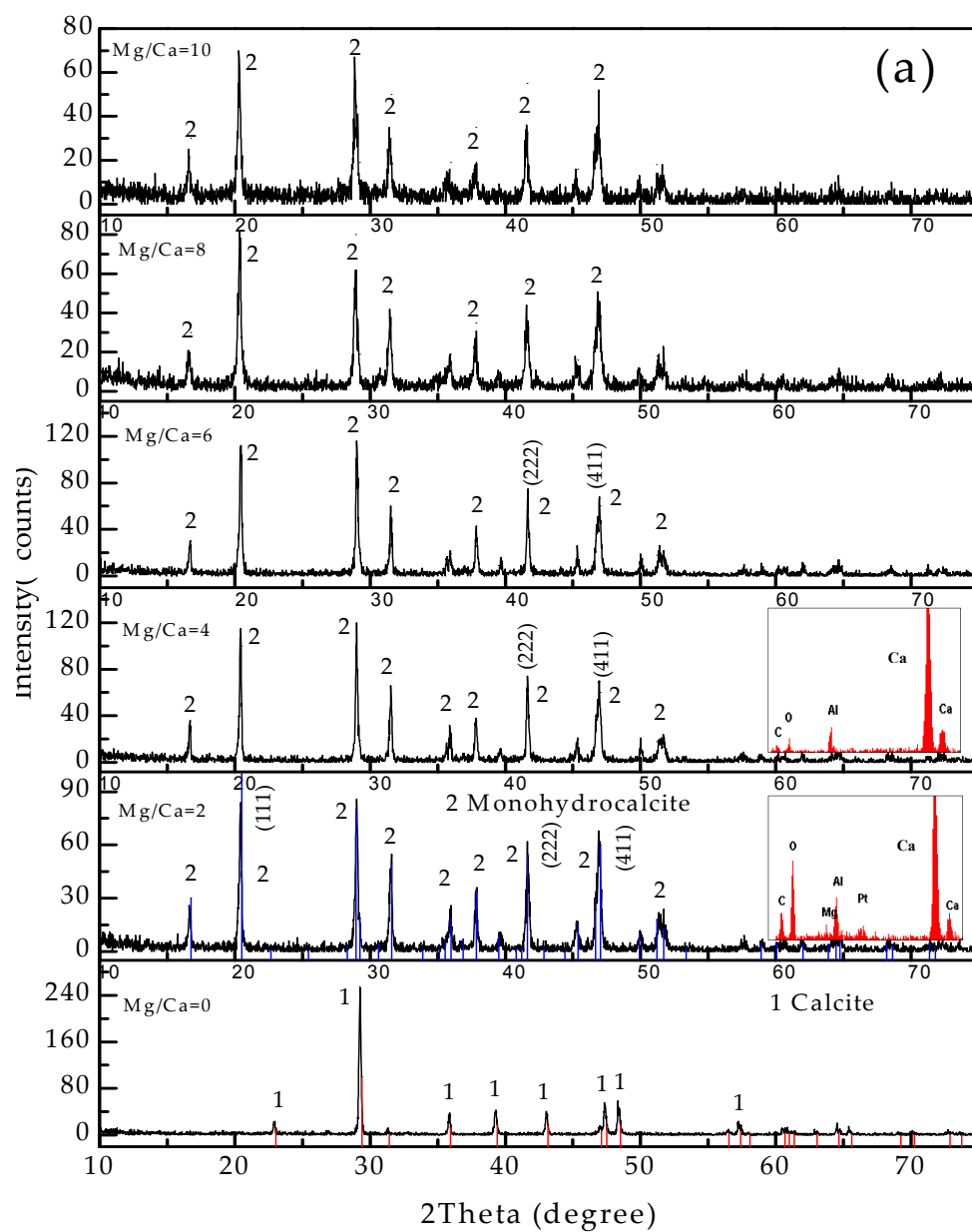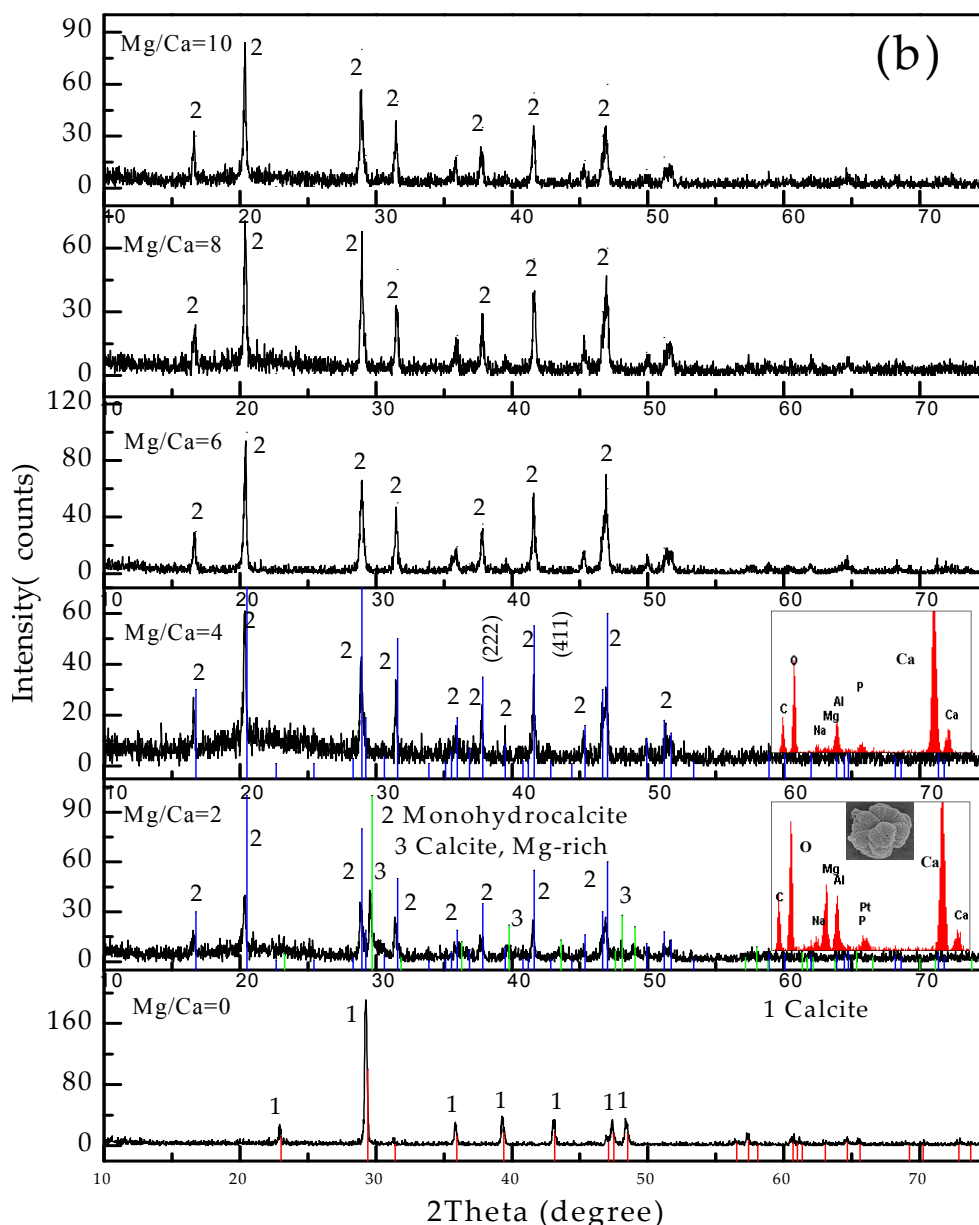
Figure 5. *Cont.*

Figure 5. XRD patterns of the minerals in $MgSO_4$ medium with 15% NaCl and different Mg/Ca molar ratios after 15 days of cultivation: (**a**) the control group; and (**b**) the experimental group. Note: The red line represents the mineral phase of calcite in PDF card 47-1743, the blue line represents the mineral phase of monohydrocalcite in PDF card 29-0306, and the green line represents the mineral phase of Mg-calcite in PDF card 43-0697.

Figure 6 shows the mineral phases and crystal surface morphology of the precipitates in the control and experimental group containing $MgCl_2$. It can be seen in Figure 6a that the mineral phase is calcite at an Mg/Ca molar ratio of 0, and monohydrocalcite at other Mg/Ca molar ratios, consistent with the results shown in Figure 5a. A small difference was noted between these two groups; that is, the mineral crystals showed a preferred orientation when $MgSO_4$ was used, whereas no such phenomenon was noted in the other group, indicating that the sources of Mg^{2+} exerted some influence on the crystal growth rate and mode. It can be seen from Figure 6b that the mineral phases are calcite at an Mg/Ca ratio of 0, Mg-rich calcite (left side of SEM) and aragonite (right side of SEM) at an Mg/Ca ratio of 2, and monohydrocalcite at other Mg/Ca ratios. These results indicate that the mineral phases were significantly different from those shown in Figure 5b. The above results demonstrate that the

source of Mg^{2+} had an important effect on the newly formed mineral phases and the appearance of preferred orientation.
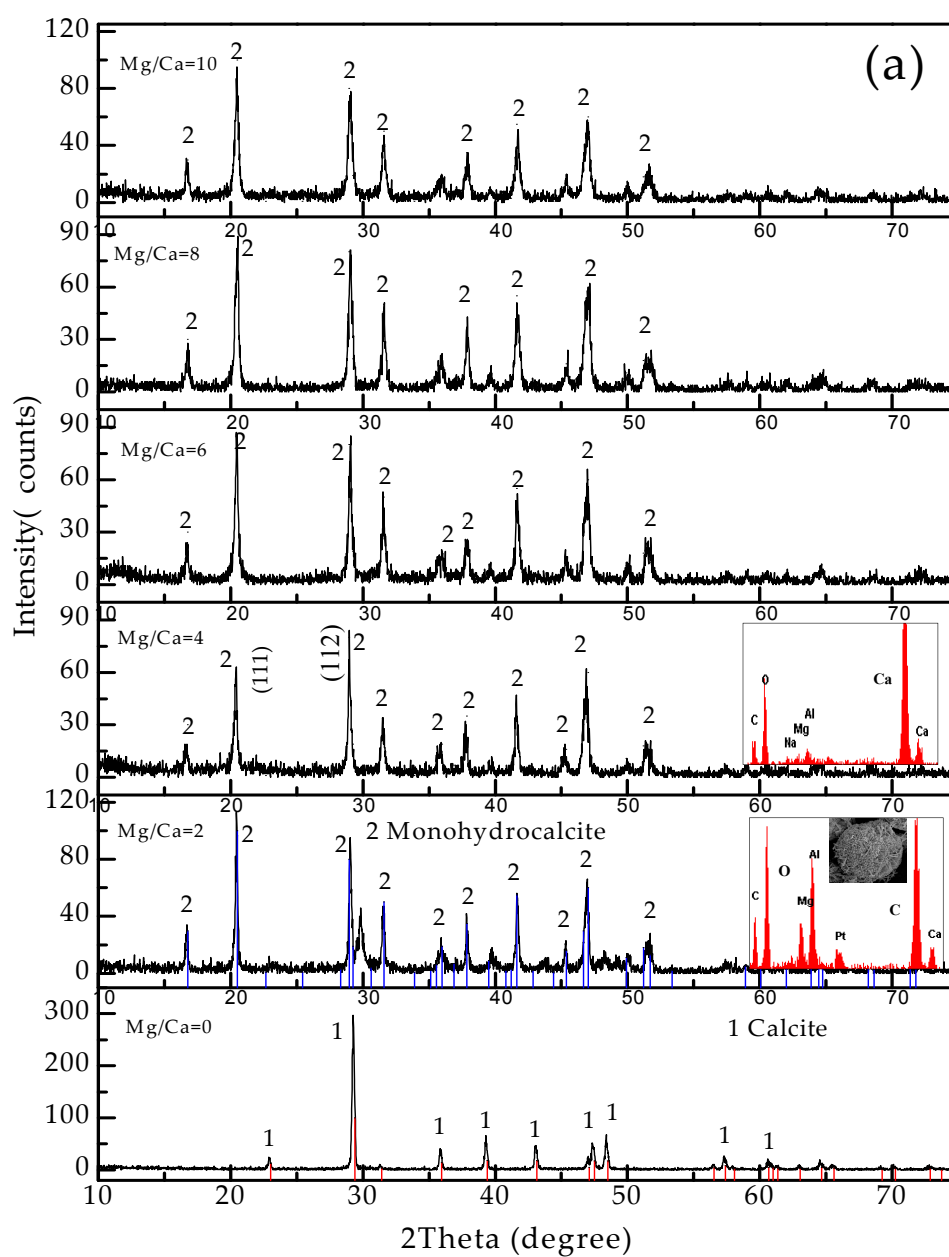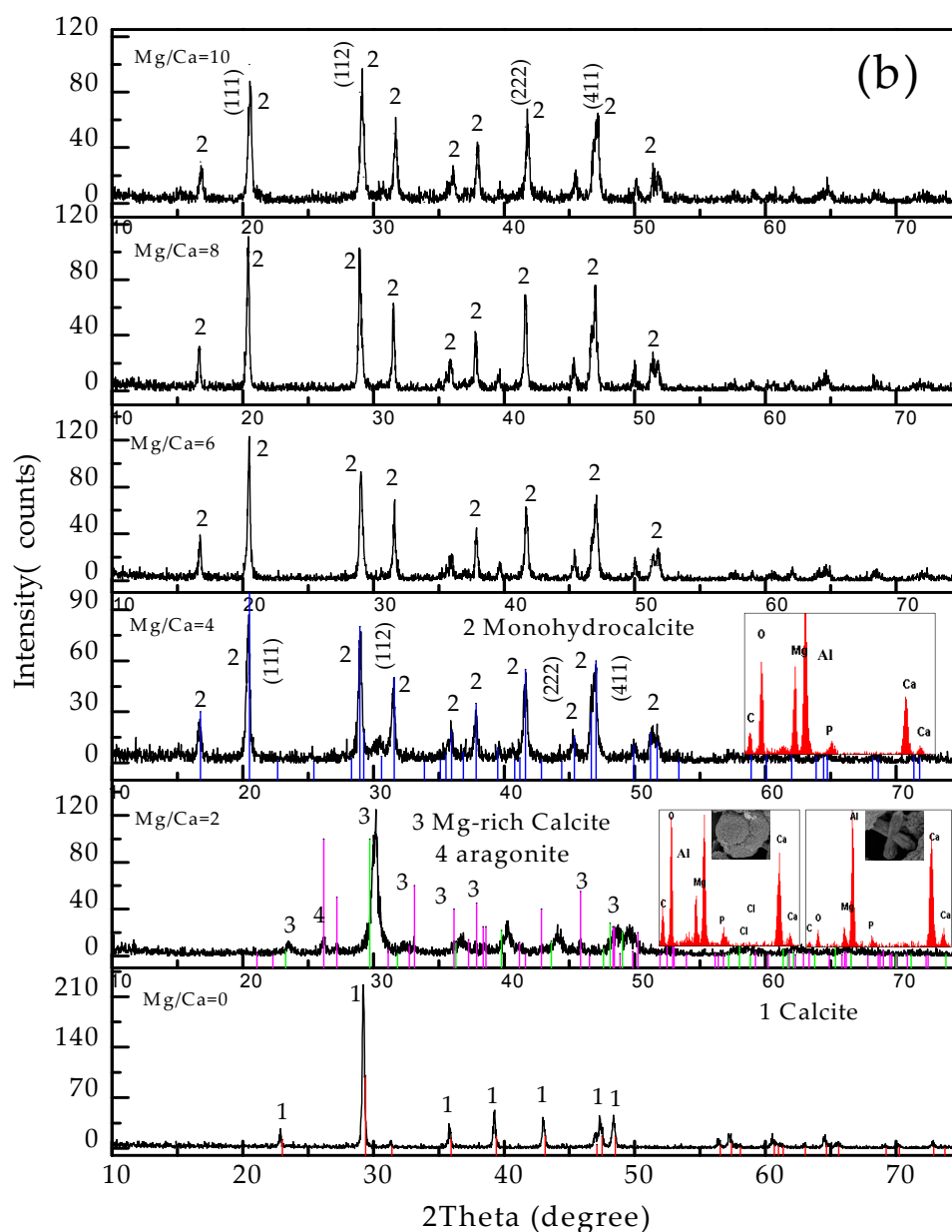

Figure 6. *Cont.*

Figure 6. XRD patterns of the minerals at 15% NaCl and different Mg/Ca molar ratios in MgCl$_2$ aqueous solution after 15 days of cultivation: (**a**) the control group; and (**b**) the experimental group. Note: The red line represents the mineral phase of calcite in PDF card 47-1743, the blue line represents the mineral phase of monohydrocalcite in PDF card 29-0306, the green line represents the mineral phase of Mg-calcite in PDF card 43-0697, and the purple line represents the mineral phase of aragonite in PDF card 41-1475.

The FTIR results of minerals in the experimental group under the condition of MgCl$_2$ solutions and Mg/Ca molar ratio of 2 are shown in Figure 7. The FTIR results in Figure 7a show the vibrational bands of different types of organic functional groups (marked by the blue arrows) and aragonite (marked by the red arrows). Figure 7b shows an enlarged view of the spectral segment in Figure 7a in the range of 2800–3000 cm^{-1}. It can be seen that C–H methylene vibrational bands (2925 cm^{-1}) and C–H methyl vibrational bands (2979 cm^{-1}) are present [42,43], indicating that the organic functional groups were involved in the formation process of these carbonate minerals.
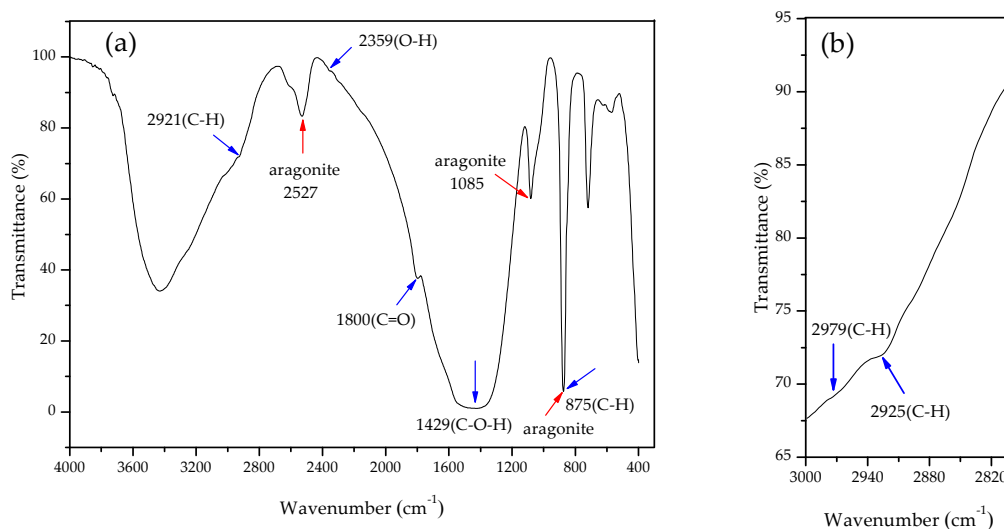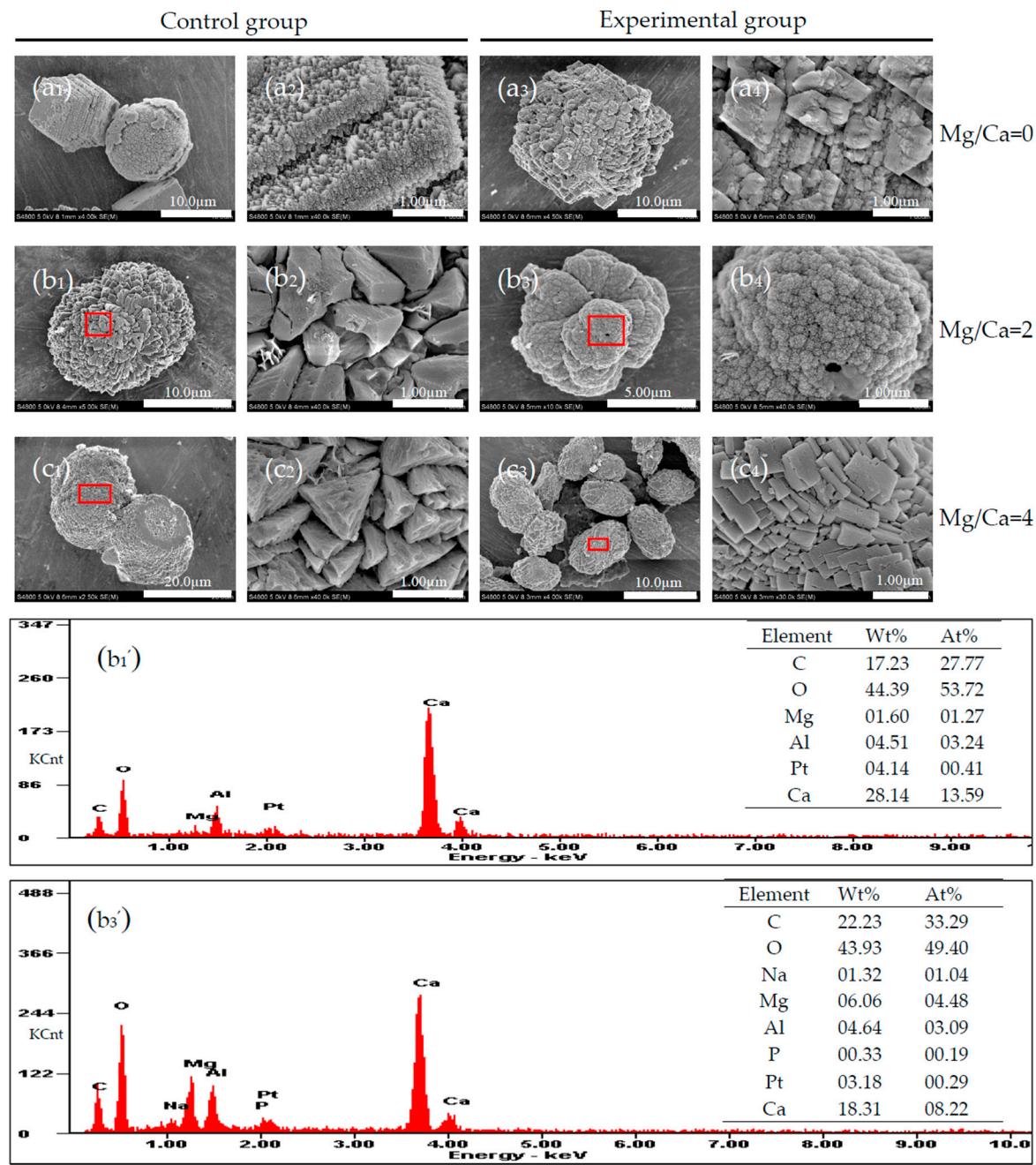
Figure 7. FTIR spectrogram of minerals formed at an Mg/Ca molar ratio of 2 in the experimental group containing $MgCl_2$: (**a**) FTIR spectrogram of minerals from 4000 cm^{-1} to 400 cm^{-1}; and (**b**) partial enlarged view of the spectrogram from 3000 cm^{-1} to 2800 cm^{-1}.

3.5. Carbonate Minerals Analyzed by SEM and EDS

To characterize micromorphological changes of minerals under different conditions, the precipitates in the control and experimental groups were analyzed using SEM and EDS. The results of the micromorphology analysis of the minerals precipitated in $MgSO_4$ solutions are shown in Figure 8. It can be seen in Figure $8a_1$ that there are two morphologies of calcite: one is rhombohedral, and the other is spherulitic. The rhombohedral calcite crystals grow in a stepwise manner, and the height of the growth step is approximately 1 μm (Figure $8a_2$). On the other hand, the calcite spherulites, which have very rough surfaces, are approximately 10 μm in diameter at an Mg/Ca ratio of 0. Figure $8b_1$ shows that the dumbbell-shaped monohydrocalcite crystals, which have a length of approximately 12–15 μm, are covered with large quantities of hedrite crystals (Figure $8b_2$) at an Mg/Ca ratio of 2. The results of EDS analysis of the mineral grains marked with a red square in Figure $8b_1{}'$ show that the main elements are Ca, C, O, Mg, Pt, and Al. Mg came from the culture medium, Pt came from the process of sample preparation in vacuum, and Al came from the upholder under the sample. The mineral grains that formed in the medium at an Mg/Ca ratio of 4 were dumbbell-shaped and 12–20 μm in length (Figure $8c_1$). Figure $8c_2$ shows that the surface of the monohydrocalcite is also covered with a large quantity of hedrite crystals, and these crystals are more regular than those shown in Figure $8b_2$. The EDS results show that the elemental composition of the mineral grains includes Ca, C, O, and small amounts of Al (Figure $8c_1{}'$). Figure $8a_3,a_4$ show the micromorphology of the calcite in the experimental group at an Mg/Ca ratio of 0, which illustrates that LD532 bacteria played an important role in the micromorphological changes. In this figure, the growth surface of calcite is generally irregular and is dominated by unclear growth steps, not rhombohedral or spherulitic forms, and their rougher surfaces are covered with different sizes of irregular crystals that are obviously different from those in the control group. The mineral grains precipitated in the culture medium at an Mg/Ca molar ratio of 2 primarily display cauliflower-shaped forms (Figure $8b_3$), and their surfaces are composed of particulate crystals (Figure $8b_4$). The elemental composition of the minerals includes Ca, C, O, and small amounts of Mg, Al, Na, and P (Figure $8b_3{}'$). P may come from LD532 bacteria. The crystals are elliptical at an Mg/Ca molar ratio of 4 (Figure $8c_3$), and the surface is covered with many flaky minerals with regular geometric shapes (Figure $8c_4$). The EDS results show that the elemental composition of these precipitates includes Ca, C, O, and small amounts of Mg, Al, Na, and P (Figure $8c_3{}'$). It can be seen in Figure 8 that there are significant differences in the morphology and elemental composition of

the mineral precipitates between the control and experimental group, indicating that LD532 bacteria played a vital role in the biomineralization process.
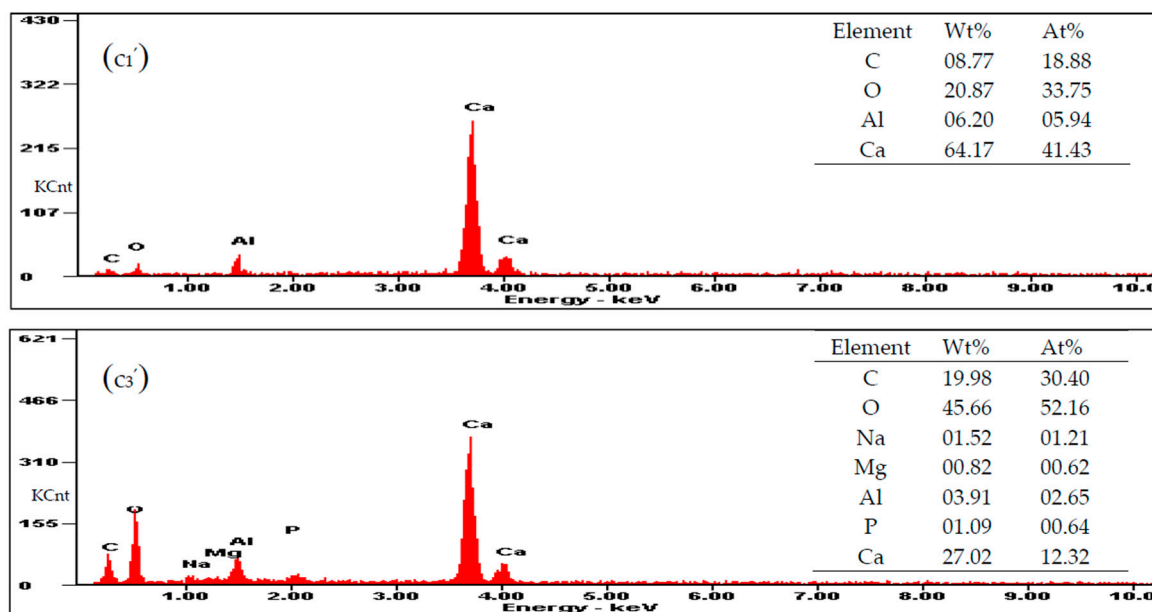

Element	Wt%	At%
C	17.23	27.77
O	44.39	53.72
Mg	01.60	01.27
Al	04.51	03.24
Pt	04.14	00.41
Ca	28.14	13.59

Element	Wt%	At%
C	22.23	33.29
O	43.93	49.40
Na	01.32	01.04
Mg	06.06	04.48
Al	04.64	03.09
P	00.33	00.19
Pt	03.18	00.29
Ca	18.31	08.22

Figure 8. *Cont.*

(c1')

Element	Wt%	At%
C	08.77	18.88
O	20.87	33.75
Al	06.20	05.94
Ca	64.17	41.43

(c3')

Element	Wt%	At%
C	19.98	30.40
O	45.66	52.16
Na	01.52	01.21
Mg	00.82	00.62
Al	03.91	02.65
P	01.09	00.64
Ca	27.02	12.32

Figure 8. SEM and EDS images of the minerals in control and experimental groups at 15% NaCl and different Mg/Ca molar ratios in $MgSO_4$ solution after 15 days of cultivation: (a_1,a_2) Mg/Ca molar ratio of 0 in the control group; (b_1,b_2) Mg/Ca molar ratio of 2 in the control group; (c_1,c_2) Mg/Ca molar ratio of 4 in the control group; (a_3,a_4) Mg/Ca molar ratio of 0 in the experimental group; (b_3,b_4) Mg/Ca molar ratio of 2 in the experimental group; (c_3,c_4) Mg/Ca molar ratio of 4 in the experimental group; and ($b_1{}'$,$b_3{}'$,$c_1{}'$,$c_3{}'$) EDS analysis of the mineral marked by the red square, respectively.

Figure 9 shows the micromorphologies of mineral precipitates formed in the culture medium with different concentrations of $MgCl_2$. Calcite at an Mg/Ca molar ratio of 0 are made up of a large number of irregular rhombohedral crystals with a length of up to about 8 μm (Figure $9a_1$), and the surfaces of calcite are composed of nanoscale particles (Figure $9a_2$). The monohydrocalcite spherules at an Mg/Ca molar ratio of 2, ranging from 8 to 12 μm in diameter (Figure $9b_1$), are composed of a large number of fibrous mineral crystals (Figure $9b_2$). EDS analysis shows that the elemental composition of this mineral includes C, O, and Ca, and small amounts of Mg, Al, and Pt (Figure $9b_1{}'$). Pt was originated from the spraying operation performed during the sample preparation process. The dumbbell-shaped monohydrocalcite shown in Figure $9c_1$, which is 15–20 μm in length, is covered with a large quantity of hedrite crystals (Figure $9c_2$) that are smaller than those in $MgSO_4$ medium. EDS results show that the elemental composition of this mineral includes Ca, C, O, and small amounts of Mg, Al, and Na (Figure $9c_1{}'$). In the experimental group, the bunchy type of calcite at an Mg/Ca molar ratio of 0 (Figure $9a_3$), approximately 5–10 μm in length, is precipitated and composed of countless smaller rhombohedral calcite crystals (Figure $9a_4$). Cross-shaped mineral precipitates can be observed in Figure $9b_3$ (marked with the yellow arrows), approximately 5 μm in length. EDS result shows that the elemental composition of this mineral includes Al, Ca, C, O, Mg, and P (Figure $9b_3{}'$). The mineral precipitates at an Mg/Ca molar ratio of 2 are approximately 5–8 μm in length, mainly cauliflower-shaped and dumbbell-shaped (Figure $9b_4$). The crystals formed in the culture medium at an Mg/Ca molar ratio of 4 are dumbbell-shaped and the sizes are approximately 5 μm in length (Figure $9c_3$). The micromorphology of this mineral shown in Figure $9c_4$ is proved that the surface is covered with a large quantity of microcrystals. EDS results show that the elemental composition of this mineral includes Ca, C, O, Mg, Al, and P (Figure $9c_3{}'$). From the above result, it could be concluded that there were significant differences in the morphology and elemental composition of the mineral precipitates between the control and experimental groups.

A comparison of the mineral precipitates in $MgSO_4$ solutions and those in $MgCl_2$ solutions shows that different sources of Mg^{2+} can affect the surface micromorphology, elemental composition, and mineral phase of the minerals induced by LD532 bacteria.

At the same time, LD532 bacteria could not be observed on the surfaces of mineral precipitates shown in Figures 8 and 9.
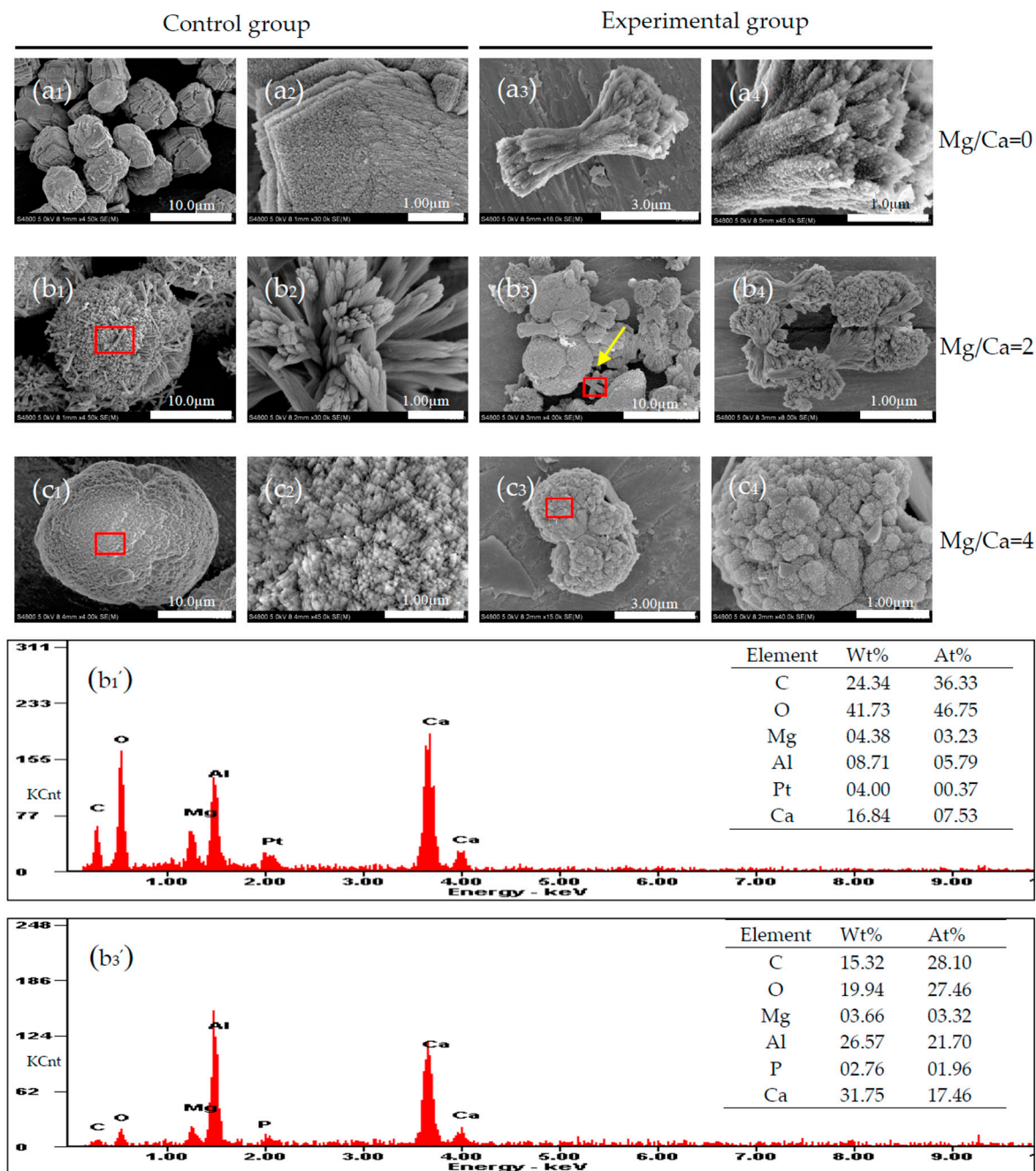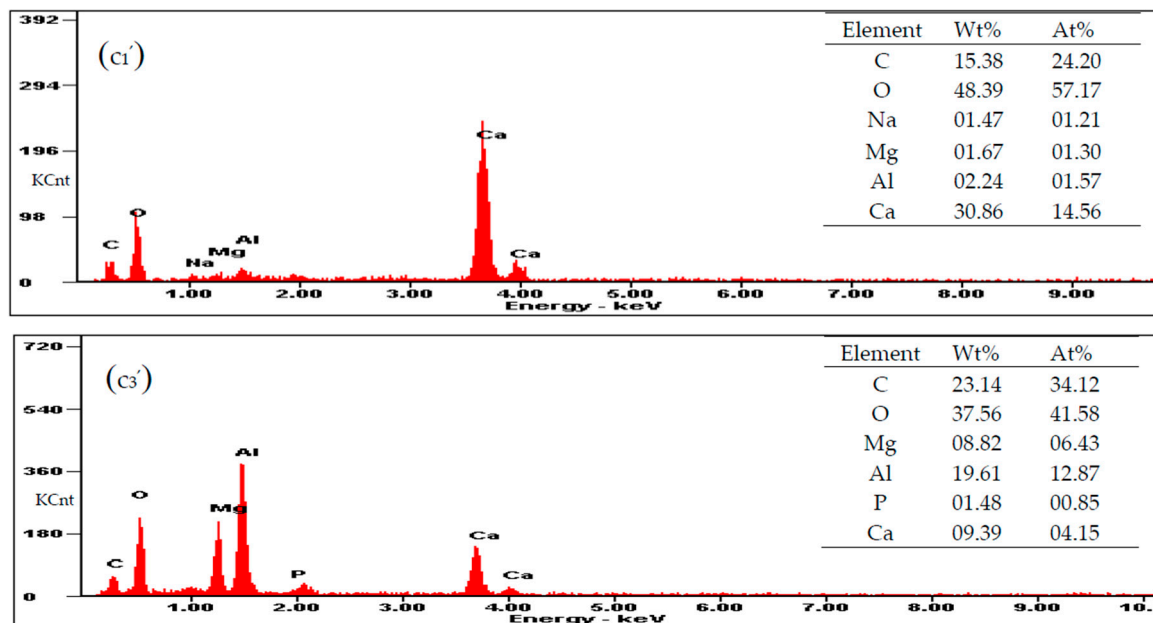

Element	Wt%	At%
C	24.34	36.33
O	41.73	46.75
Mg	04.38	03.23
Al	08.71	05.79
Pt	04.00	00.37
Ca	16.84	07.53

Element	Wt%	At%
C	15.32	28.10
O	19.94	27.46
Mg	03.66	03.32
Al	26.57	21.70
P	02.76	01.96
Ca	31.75	17.46

Figure 9. *Cont.*

Figure 9. SEM and EDS images of the minerals in control and experimental groups at 15% NaCl and different Mg/Ca molar ratios in $MgCl_2$ solution after 15 days of cultivation: (**a$_1$,a$_2$**) Mg/Ca molar ratio of 0 in the control group; (**b$_1$,b$_2$**) Mg/Ca molar ratio of 2 in the control group; (**c$_1$,c$_2$**) Mg/Ca molar ratio of 4 in the control group; (**a$_3$,a$_4$**) Mg/Ca molar ratio of 0 in the experimental group; (**b$_3$,b$_4$**) Mg/Ca molar ratio of 2 in the experimental group; (**c$_3$,c$_4$**) Mg/Ca molar ratio of 4 in the experimental group; and (**b$_1$′,b$_3$′,c$_1$′,c$_3$′**) EDS analysis of the mineral marked by the red square, respectively.

3.6. Nucleation Sites of Minerals on the EPS of C. israelensis LD532 Bacteria

To determine the nucleation sites of the carbonate minerals, *C. israelensis* LD532 bacteria at an Mg/Ca ratio of 2 in $MgSO_4$ and $MgCl_2$ aqueous solutions were analyzed with HRTEM. Figure 10a$_1$ shows the micromorphology of *C. israelensis* LD532 bacteria, indicating that the cell surfaces were covered with different sizes of particulates. It can be seen from Figure 10b$_1$,c$_1$ that these particulates have a definite crystal structure, based on the halo ring and the bright spot in the SAED figures, and NaCl crystals can be determined by the EDS analysis. Only minor amounts of elements Mg and Ca have been measured on the surface of *C. israelensis* LD532 bacteria, indicating that EPS may have provided the nucleation sites for these carbonate minerals in $MgSO_4$ aqueous solutions. Figure 10a$_2$,b$_2$ shows that large quantities of microcrystals cover the surface of *C. israelensis* LD532 bacteria, while Figure 10c$_2$ shows that these microcrystals are mainly composed of Na and Cl elements, only minor amounts of Mg and Ca, and therefore the minerals on the EPS were mainly NaCl in $MgCl_2$ aqueous solutions. The existence of Mg, Ca, C, and O may suggest that tiny crystals may be nucleated on the EPS.

To further prove the nucleation sites of the carbonate minerals, ultra-thin slices of *C. israelensis* LD532 bacteria grown in $MgSO_4$ and $MgCl_2$ aqueous solutions were prepared and observed by TEM. The results are shown in Figure 11. Figure 11a$_1$–c$_1$ show images of the ultra-thin slices of *C. israelensis* LD532 bacteria grown in $MgSO_4$ solutions, and Figure 11a$_2$–c$_2$ show images of the ultra-thin slices of *C. israelensis* LD532 bacteria grown in $MgCl_2$ solutions. It can be obtained from Figure 11 that minerals with a size of dozens of nanometers can be formed in the EPS and at some intracellular sites (marked with yellow arrows), suggesting that biomineralization can occur either in the cell or outside the cell. These minerals may be carbonates because NaCl crystals could not form inside the cells of halophilic bacteria, otherwise, the survival of halophiles could be threatened, what was more, halophiles had been washed many times with PBS solution in order to remove the residual NaCl during the preparation of ultra-thin slices. From the above results, it can be concluded that the nucleation sites of minerals were

located on the EPS and the membrane of intracellular vesicles of *C. israelensis* LD532 bacteria in the $MgSO_4$ and $MgCl_2$ solutions. Of course, it would be better to examine them by TEM with EDS and SAED. This content will be reported continually in future studies.
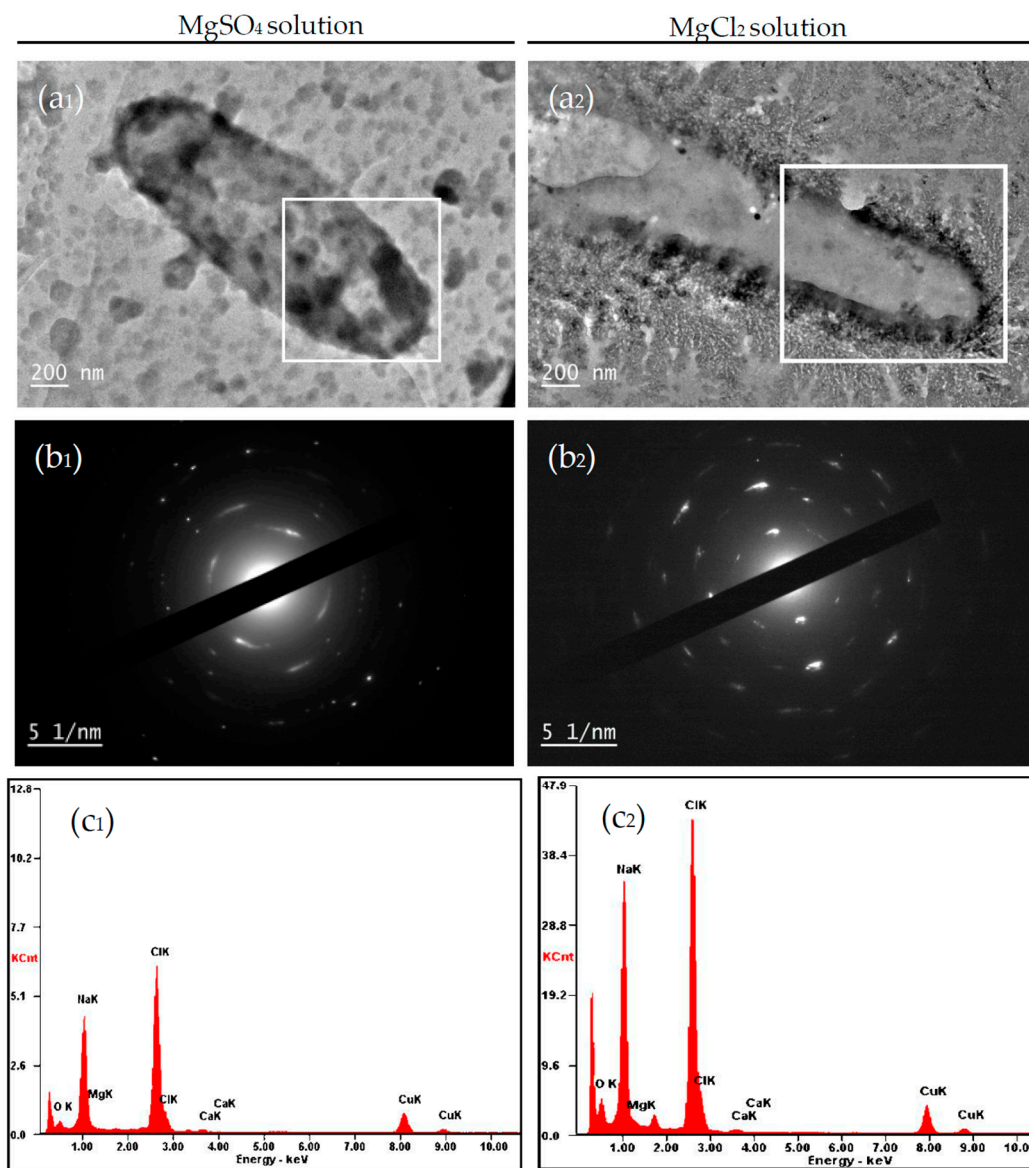

Figure 10. HRTEM, SAED, and EDS analysis of LD532 bacteria cell: (**a₁**) HRTEM analysis of LD532 bacteria cell at an Mg/Ca ratio of 2 in $MgSO_4$ solution; (**b₁,c₁**) SAED and EDS analyses of LD532 bacteria cell marked by the white square; (**a₂**) HRTEM analysis in the experimental group at Mg/Ca molar ratio of 2 in $MgCl_2$ aqueous solution; and (**b₂,c₂**) SAED and EDS analyses of LD532 bacteria cell marked by the white square.
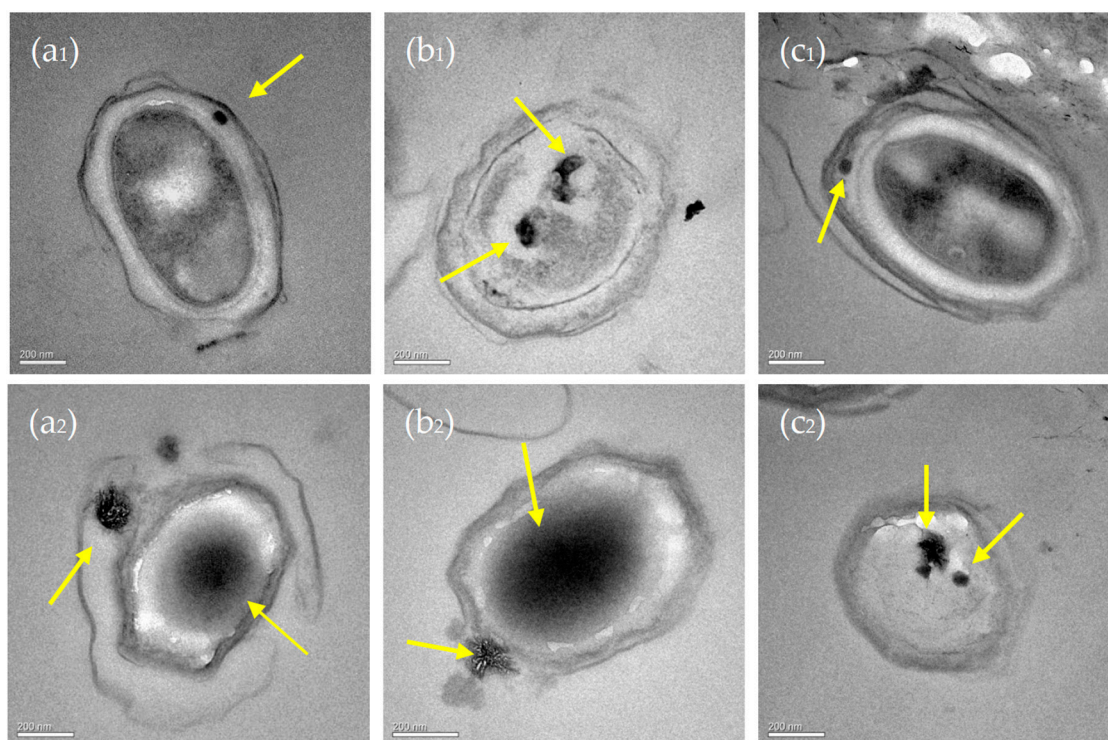
Figure 11. TEM images of ultrathin slices of LD532 bacterial cell after 30 days of culture: (a_1–c_1) TEM analyses of cells at an Mg/Ca ratio of 2 in $MgSO_4$ solution; and (a_2–c_2) TEM analyses of cells at an Mg/Ca ratio of 2 in $MgCl_2$ solution. The intracellular and extracellular minerals are marked with yellow arrows.

4. Discussion

4.1. The Mechanism of Biomineralization Induced by C. israelensis LD532 Bacteria

Certain types of microorganisms can release enormous amounts of CA via metabolism activity, which can change the ambient pH values in appropriate surroundings [44]. The activity of CA has been found in a wide range of microorganisms and plants. CA produced by bacterial metabolic activity also plays an extremely important role in the biomineralization process [21,22,44,45] partly due to the fact that this enzyme promotes carbon dioxide and water to react to produce bicarbonate, which can increase the pH values in the culture medium, and thus prerequisite conditions for the precipitation of minerals can be provided. In this work, CA secreted by *C. israelensis* LD532 bacteria was also found. CA is a ubiquitous metalloenzyme that can catalyze the reversible hydration reaction of CO_2 [20]. CA can eliminate dynamic obstacles and plays an important catalytic role in promoting the conversion of inorganic carbon [24]. The conversion between CO_2 and HCO_3^- can be catalyzed by this enzyme, and the conversion formula is displayed as Equation (1).

$$CO_2 + H_2O \leftrightarrow HCO_3^- + H^+ \qquad (1)$$

Inorganic carbon exists in the form of carbon dioxide and carbonic acid in the acidic solution, while it can be present in the form of bicarbonate and carbonate under alkaline conditions. More importantly, higher CA activity of *C. israelensis* LD532 bacteria in alkaline solutions (pH values of approximately 8.8) was conspicuous, which is shown in Figure 4b,c, indicating that more and more bicarbonate ions were released to facilitate the following chemical reaction:

$$Ca^{2+} + 2HCO_3^- \rightarrow CaCO_3 \downarrow + H_2O + CO_2 \uparrow \qquad (2)$$
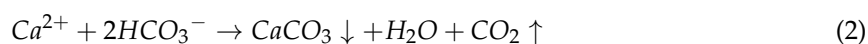
CA plays an important role in the biomineralization of carbonate. CA occurs widely and participates in the process of converting CO_2 into HCO_3^-, transportation of acid and ion, and cellular pH regulation [44]. CA enzyme catalyzes the reversible hydration of CO_2, HCO_3^- can be released in alkaline condition under the catalysis of this enzyme, then react with Ca^{2+} to produce calcium carbonate precipitates, which can explain the mechanism of carbonate precipitation induced by *H. anticariensis* [33]. In this study, CA released from *C. israelensis* LD532 bacteria also promoted the biomineralization of calcium carbonate, and the mechanism of biomineralization was similar with the above.

In this study, the physiological and biochemical identification experiments show that ammonia can be released by LD532 bacteria (Table 1). According to Equation (3), it can be concluded that ammonia tends to increase the pH of its environment.

$$NH_3 + H_2O \rightarrow NH_4^+ + OH^- \tag{3}$$

The increase in pH values shown in Figure 4c was due to the above reaction. The carbonic acid produced could be converted into HCO_3^- under alkaline conditions and the catalysis effect of CA. Therefore, chemical Reaction (4) occurred in the solution:

$$Ca^{2+} + HCO_3^- + OH^- \rightarrow CaCO_3 \downarrow + H_2O \tag{4}$$
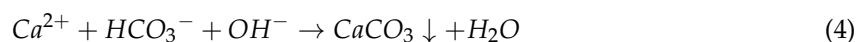
Our experimental conclusions indicated that the alkaline condition formed in the culture medium was a prerequisite for the biomineralization of calcium carbonate. They were also consistent with previous results [4,46]. According to the above reaction, it can be easily known that the process of calcium carbonate biomineralization occurred mainly according to Reaction (4), indicating that CA and ammonia released by *C. israelensis* LD532 bacteria played a key role in this process.

4.2. Influence of Mg^{2+} Source, Concentration and Bacterial Strain on Carbonate Minerals

4.2.1. Carbonate Minerals in $MgSO_4$ and $MgCl_2$ Solutions

In this study, the minerals Mg-calcite and monohydrocalcite were precipitated in the experimental group at an Mg/Ca molar ratio of 2 in $MgSO_4$ solutions, whereas only the mineral monohydrocalcite was observed in the control group. The minerals Mg-calcite and a small quantity of aragonite were found at the same Mg/Ca molar ratio in $MgCl_2$ solution in the experimental group, whereas only the mineral monohydrocalcite was obtained in the control group. Many researchers have confirmed that bacteria can modify the chemical composition of the culture medium and create appropriate microenvironments to favor the precipitation of carbonate minerals [20,47,48]. The mineral phases in these two experimental groups were different (Figures 5b and 6b) because the environments for bacterial growth were different: one was $MgSO_4$ solution and the other was $MgCl_2$ solution. It has been reported that Mg^{2+} can damage the crystal growth of calcite because Ca atoms can be replaced by Mg atoms. Therefore, the (104) diffraction peak of calcite shifted to the right, as shown in Figures 5b and 6b, and Mg-calcite formed. The formation of Mg-calcite in $MgSO_4$ and $MgCl_2$ solutions at an Mg/Ca molar ratio of 2 occurred according to the above principle. On the other hand, another mineral, aragonite, formed in $MgCl_2$ solutions but not $MgSO_4$ solutions, perhaps because the calcite was dissolved and recrystallized in the $MgCl_2$ solutions. The formation of ion pairs between SO_4^{2-} and Mg^{2+} may have reduced the replacement of Ca atoms by Mg atoms, resulting in the dissolution and recrystallization of calcite could not occur in the $MgSO_4$ solutions, and therefore no aragonite crystals formed. Based on the above analysis, it can be seen that the different sources of Mg^{2+} and LD532 bacteria played very important roles in the formation of new minerals during the biomineralization process.

4.2.2. Morphology of Carbonate Minerals

Combined with the XRD and FTIR analyses, Mg-rich calcite and small amounts of aragonite formed in the experimental group at an Mg/Ca molar ratio of 2 in $MgCl_2$ solutions, while monohydrocalcite formed in the control group. Therefore, the surface morphology of minerals was different because of their different mineral phases. Significant differences in the surface morphology of minerals formed between the experimental and control group could be observed (Figure $9b_1$–b_4). The organic macromolecules of organisms play an important role in regulating and controlling the formation of the unique morphology of the minerals in the biomineralization process [41]. Organic functional groups have some influence on the morphology of calcite [34]. In our experimental study, the organic functional groups, such as O–H, C=O, C–H methylene, and C–H methyl (Figure 7a,b), played an important role in regulating and controlling the morphology of minerals.

The morphology of monohydrocalcite induced by different strains and different conditions was variable. In our research, the morphology of monohydrocalcite induced by *C. israelensis* LD532 bacteria was also different under different growth conditions (Figures 8 and 9). The monohydrocalcite formed in $MgSO_4$ solutions (Figure $8b_1,c_1$) was mainly dumbbell-shaped, and the surfaces were also covered with large quantities of regular or irregular hedrite crystals; however, the monohydrocalcite formed in $MgCl_2$ solutions (Figure $9b_1,c_1$) was mainly spherulitic and elliptical, and the surface was composed of a large number of fibrous mineral crystals and smaller hedrite crystals. Mg^{2+} plays a very important role in the formation process of monohydrocalcite. Many researchers have reported that Mg is ubiquitous in the formation of monohydrocalcite in both laboratory experiments and natural environments [49,50], and a high content of Mg in the culture medium is a prerequisite for its formation [51]. It was clear that the difference in mineral morphology was caused by the different sources of Mg^{2+} because the bacteria were not present and the other conditions were the same as those in the process of biomineralization. The morphology of calcite and monohydrocalcite induced by *C. israelensis* LD532 bacteria was also different at the same Mg/Ca molar ratio and the same source of Mg^{2+} in the experimental groups, indicating that the biological activity of *C. israelensis* LD532 bacteria can alter the surface morphology of these minerals.

In this study, it was concluded that the surface morphology of the minerals induced by *C. israelensis* LD532 bacteria had changed, new mineral phases appeared during the process of biomineralization, and Mg/Ca ratios and the source of Mg^{2+} in the solution also controlled the crystal morphology, mineral phase, and elemental composition of the minerals.

4.3. The Formation of Aragonite in the Presence of C. israelensis LD532 Bacteria

The results of XRD (Figure 6b) and SEM (Figure $9b_3$) show that aragonite was precipitated at an Mg/Ca molar ratio of 2 in the experimental group containing $MgCl_2$ solution, whereas no aragonite was precipitated in the control group. The result of EDS shows that the elemental composition of the aragonite includes Al, Ca, C, O, Mg, and P (Figure $9b_3{}'$). Al came from the upholder under the sample, Mg was derived from the culture medium, and P might be derived from LD532 bacteria. The shape of aragonite formed in this study was consistent with cross-shaped aragonite observed using a polarizing microscope [52]. It has been reported that Mg^{2+} can hardly be detected in non-biogenic aragonite minerals [53] because Mg^{2+} does not enter the orthorhombic aragonite lattice, however, aragonite formed by biological processes often contains Mg^{2+}. The elemental composition of aragonite determined using EDS included Mg element in this study, indicating that *C. israelensis* LD532 bacteria may have an important controlling effect on the Mg content of aragonite.

4.4. Intracellular and Extracellular Biomineralization of Carbonate Minerals

Bacteria can change their ambient environments [30] and provide nucleation sites by adsorbing Ca^{2+}, Mg^{2+}, and other metallic cations onto EPS, membranes, and cell walls [23,54] in the precipitation process of minerals. The EPS produced by bacteria not only plays a vital role in the overall ionic charges,

it also serves as a nucleation site during the process of calcification [13]. It can be seen from Figure 11 that biomineralization can occur in the intracellular and extracellular LD532 bacteria, indicating that the nucleation sites may be on the EPS and the membranes of intracellular vesicles. Bacteria can serve as a nucleus for carbonate mineral precipitation by absorbing cations around their EPS [23]. The formation and structures of carbonate crystals induced by Methanogenic archaea are controlled by the cell walls and EPS [55]. EPS plays an important role in the complex process of bacterial adhesion to minerals [56,57]. Meanwhile, our experimental results were consistent with the above conclusions. EPS are mostly composed of polysaccharides (exopolysaccharides) and proteins, but they also include other macro-molecules, such as DNA, lipids, and humic substances [58], specialized measures are required to identify and quantify EPS substances definitively [59]. In this study, the pH values were above 7.3 at the start of cultivation and increased with incubation time, as shown in Figure 4c, indicating that biomacromolecules, such as proteins and DNA, were negatively charged in the alkaline environment. Therefore, the positively charged Ca^{2+} and Mg^{2+} could be absorbed on these negatively charged biomacromolecules on the EPS, and nucleation occurred subsequently. The presence of P element in Figures 8b$_3'$,c$_3'$ and 9b$_3'$,c$_3'$ shows that the mineral contained P element, indicating that there was a close relationship between the bacterially induced minerals and biomacromolecules, such as phospholipids and DNA, because there were too many phosphate groups in the phospholipids and DNA molecules. Therefore, it could be inferred from Figure 8b$_3'$,c$_3'$, Figure 9b$_3'$,c$_3'$, and Figure 11 that the nucleation sites of biomineralizaiton might occur on the phospholipids and DNA molecules located in the EPS and the intracellular vesicles. There have been many important reports that the nucleation sites of bacterially induced minerals are located on the EPS.

It was found that no bacteria were present on the surface of the minerals shown in Figures 8 and 9, which was because *C. israelensis* LD532 bacteria long soaked in anhydrous ethanol solution without any NaCl component were destroyed and lysed in the process of sample preparation for SEM. For the halophilic bacteria, Na^+ has an important role in maintaining the structure and function of cell membranes and cell walls [60]. The Na^+ present on the cytoderm of halophilic bacteria could prevent the cytoderm from lysing and could also protect the negatively charged proteins of these bacterial cells from being damaged. When the amount of Na^+ was insufficient or became diluted in the solution, the cytoderm would lyse due to the change in osmotic pressure. The negatively charged proteins would then lose their activity, and therefore the halophilic bacteria could not live any longer below a certain concentration of NaCl. Based on the above analysis, the lack of bacteria in the SEM images could be explained.

Studying the formation processes of carbonate minerals at different Mg/Ca molar ratios and exploring the mechanism of bacterially induced biomineralization is helpful for explaining their role in ancient biogeochemical cycles and reconstructing palaeoenvironments during geological history. It is also helpful to explain the origin of carbonate rocks in ancient sedimentary environments, and it is of great significance for studying the chemical evolution and early evolution of life in palaeoceanographic environments during Earth's history.

5. Conclusions

To study the effect of microbes, mainly halophiles, on the formation of mineral deposits, *C. israelensis* LD532 isolated from the Yinjiashan Saltern in China was used to investigate the biomineralization process of the carbonate minerals at different Mg/Ca molar ratios and different sources of Mg^{2+}. The activity of CA played an extremely important role in the process of biomineralization. Both intracellular and extracellular biomineralization occurred on LD532 bacteria, and the nucleation sites occurred on the EPS and the membranes of intracellular vesicles. There were significant differences in the phases and morphologies of minerals formed in $MgSO_4$ solutions and those formed in $MgCl_2$ solutions, indicating that different sources of Mg^{2+} could affect the physiological and biochemical activities of microorganisms and thereby affect the mineral deposition.

Author Contributions: Zuozhen Han conceived and designed the experiments; Dan Li and Peiyuan Li performed the experiments; Zuozhen Han, Hui Zhao, and Huaxiao Yan analyzed the results of all the experiments; Dan Li and Huaxiao Yan wrote the paper; and Hui Zhao revised the manuscript. All authors read and approved the manuscript.

Conflicts of Interest: The authors declare no conflict of interest.

References

1. Spötl, C.; Fairchild, I.J.; Tooth, A.F. Cave air control on dripwater geochemistry, Obir Caves (Austria): Implications for speleothem deposition in dynamically ventilated caves. *Geochim. Cosmochim. Acta* **2005**, *69*, 2451–2468. [CrossRef]

2. Morita, R.Y. Calcite precipitation by marine bacteria. *Geomicrobiol. J.* **1980**, *2*, 63–82. [CrossRef]

3. Ferris, F.G.; Fyfe, W.S.; Beveridge, T.J. Bacteria as nucleation sites for authigenic minerals in a metal-contaminated lake sediment. *Chem. Geol.* **1987**, *63*, 225–232. [CrossRef]

4. Castanier, S.; Le M'etayer-Levrel, G.; Perthuisot, J.P. Ca-carbonate precipitation and limestone genesis—The microbiologist point of view. *Sediment. Geol.* **1999**, *126*, 9–23. [CrossRef]

5. Rivadeneyra, M.A.; Delgado, G.; Ramos-Cormenzana, A.; Delgado, R. Biomineralization of carbonates by *Halomonas eurihalina* in solid and liquid media with different salinities: Crystal formation sequence. *Res. Microbiol.* **1998**, *149*, 277–287. [CrossRef]

6. Rivadeneyra, M.A.; Párraga, J.; Delgado, R.; Ramos-Cormenzana, A.; Delgado, G. Biomineralization of carbonates by *Halobacillus trueperi* in solid and liquid media with different salinities. *FEMS Microbiol. Ecol.* **2004**, *48*, 39–46. [CrossRef] [PubMed]

7. Rivadeneyra, M.A.; Martín-Algarra, A.; Sánchez-Navas, A.; Martín-Ramos, D. Carbonate and phosphate precipitation by Chromohalobacter marismortui. *Geomicrobiol. J.* **2006**, *23*, 89–101. [CrossRef]

8. Rivadeneyra, M.A.; Martín-Algarra, A.; Sánchez-Román, M.; Sánchez-Navas, A.; Martín-Ramos, J.D. Amorphous Ca-phosphate precursors for Ca-carbonate biominerals mediated by Chromohalobacter marismortui. *ISME J.* **2010**, *4*, 922–932. [CrossRef] [PubMed]

9. Van Lith, Y.; Warthmann, R.; Vasconcelos, C.; Mckenzie, J.A. Sulphate-reducing bacteria induce low-temperature Ca-dolomite and high Mg-calcite formation. *Geobiology* **2003**, *1*, 71–79. [CrossRef]

10. Sánchez-Román, M.; Rivadeneyra, M.A.; Vasconcelos, C.; McKenzie, J.A. Biomineralization of carbonate and phosphate by moderately halophilic bacteria. *FEMS Microbiol. Ecol.* **2007**, *61*, 273–284. [CrossRef] [PubMed]

11. Ehrlich, H.L. *Geomicrobiology*, 4th ed.; (Revised and Expanded); Marcel Dekker: New York, NY, USA, 2002.

12. Kranz, S.A.; Wolf-Gladrow, D.; Nehrke, G.; Langer, G.; Rost, B. Calcium carbonate precipitation induced by the growth of the marine cyanobacteria Trichodesmium. *Limnol. Oceanogr.* **2010**, *55*, 2563–2569. [CrossRef]

13. Braissant, O.; Decho, A.W.; Dupraz, C.; Glunk, C.; Przekop, K.M.; Visscher, P.T. Exopolymeric substances of sulfate-reducing bacteria: Interactions with calcium at alkaline pH and implication for formation of carbonate minerals. *Gebiology* **2007**, *5*, 401–411. [CrossRef]

14. Han, Z.Z.; Zhao, Y.Y.; Yan, H.X.; Zhao, H.; Han, M.; Sun, B.; Sun, X.Y.; Hou, F.F.; Sun, H.; Han, L.; et al. Struvite Precipitation Induced by a Novel Sulfate-Reducing Bacterium Acinetobacter calcoaceticus SRB4 Isolated from River Sediment. *Geomicrobiol. J.* **2015**, *32*, 868–877. [CrossRef]

15. Ercole, C.; Cacchio, P.; Botta, A.L.; Centi, V.; Lepidi, A. Bacterially induced mineralization of calcium carbonate: The role of exopolysaccharides and capsular polysaccharides. *Microsc. Microanal.* **2007**, *13*, 42–50. [CrossRef] [PubMed]

16. Han, Z.Z.; Yan, H.X.; Zhou, S.X.; Zhao, H.; Zhang, Y.; Zhang, N.N.; Yao, C.K.; Zhang, L.; Han, C.Y. Precipitation of calcite induced by *Synechocystis* sp. PCC6803. *World J. Microbiol. Biotechnol.* **2013**, *29*, 1801–1811. [CrossRef] [PubMed]

17. Yan, H.X.; Han, Z.Z.; Zhao, H.; Zhou, S.X.; Chi, N.J.; Han, M.; Kou, X.Y.; Zhang, Y.; Xu, L.L.; Tian, C.C.; et al. Characterization of calcium deposition induced by *Synechocystis* sp. PCC6803 in BG11 culture medium. *Chin. J. Oceanol. Limnol.* **2014**, *32*, 503–510. [CrossRef]

18. Boquet, E.; Boronat, A.; Ramos-Cormenzana, A. Production of calcite (calcium carbonate) crystals by soil bacteria is a general phenomenon. *Nature* **1973**, *246*, 527–529. [CrossRef]

19. Lowenstam, H.A.; Weiner, S. *On Biomineralization*; Oxford University Press: Oxford, UK, 1989.

20. Dhami, N.K.; Mukherjee, A.; Reddy, M.S. Micrographical minerological and nano-mechanical characterisation of microbial carbonates from urease and carbonic anhydrase producing bacteria. *Ecol. Eng.* **2016**, *94*, 443–454. [CrossRef]

21. Lian, B.; Hu, Q.N.; Chen, J.; Ji, J.F.; Teng, H.H. Carbonate biomineralization induced by soil bacterium Bacillus megaterium. *Geochim. Cosmochim. Acta* **2006**, *70*, 5522–5535. [CrossRef]

22. Braissant, O.; Cailleau, G.; Dupraz, C.; Verrecchia, E.P. Bacterially induced mineralization of calcium carbonate in terrestrial environment: The role of exopolysaccharides and amino-acids. *J. Sediment. Res.* **2003**, *73*, 485–490. [CrossRef]

23. Van Lith, Y.; Warthmann, R.; Vasconcelos, C.; Mckenzie, J.A. Microbial fossilization in carbonate sediments: A result of the bacterial surface involvement in dolomite precipitation. *Sedimentology* **2003**, *50*, 237–245. [CrossRef]

24. Han, Z.Z.; Zhao, Y.Y.; Yan, H.X.; Zhao, H.; Han, M.; Sun, B.; Meng, R.R.; Zhuang, D.X.; Li, D.; Gao, W.J.; et al. The Characterization of Intracellular and Extracellular Biomineralization Induced by *Synechocystis* sp. PCC6803 Cultured under Low Mg/Ca Ratios Conditions. *Geomicrobiol. J.* **2016**, *34*, 362–373. [CrossRef]

25. Sen, S.; Ingale, S.L.; Kim, Y.W.; Kim, K.H.; Khong, Y.W.; Lohakare, J.D.; Kim, E.K.; Kim, H.S.; Ryu, M.H.; Kwon, I.K.; et al. Effect of supplementation of Bacillus subtilis LS 1–2 to broiler diets on growth performance, nutrient retention, caecal microbiology and small intestinal morphology. *Res. Vet. Sci.* **2012**, *93*, 264–268. [CrossRef] [PubMed]

26. Cailleau, G.; Braissant, O.; Dupraz, C.; Aragno, M.; Verrecchia, E.P. Biologically induced accumulation of $CaCO_3$ in orthox soils of Biga. *Catena* **2005**, *59*, 1–17. [CrossRef]

27. Rivadeneyra, M.A.; Delgado, R.; Parraga, J.; Ramos-Cormenzana, A.; Delgado, G. Precipitation of Minerals by 22 Species of Moderately Halophilic Bacteria in Artificial Marine Salts Media: Influence of Salt Concentration. *Folia Microbiol.* **2006**, *51*, 445–453. [CrossRef]

28. Taylor, S.R.; Mclennan, S.M. *The Continental Crust: Its Evolution and Composition*; Blackwell Science: Oxford, UK, 1985.

29. Stanley, S.M.; Ries, J.B.; Hardie, L.A. Low-magnesium calcite produced by coralline algae in seawater of Late Cretaceous composition. *Proc. Natl. Acad. Sci. USA* **2002**, *99*, 15323–15326. [CrossRef] [PubMed]

30. Sánchez-Román, M.; Romanek, C.S.; Fernández-Remolar, D.C.; Sánchez-Navas, A.; McKenzie, J.A.; Pibernat, R.A.; Vasconcelos, C. Aerobic biomineralization of Mg-rich carbonates: Implications for natural environments. *Chem. Geol.* **2011**, *281*, 143–150. [CrossRef]

31. Rodriguez-Blanco, J.D.; Shaw, S.; Bots, P.; Roncal-Herrero, T.; Benning, L.G. The role of Mg in the crystallization of monohydrocalcite. *Geochim. Cosmochim. Acta* **2014**, *127*, 204–220. [CrossRef]

32. Ventosa, A.; Gutierrez, M.C.; Garcia, M.T.; Ruiz-Berraquero, F. Classification of "Chomobacterium marismortui" in a New Genus, Chromohalobacter gen. nov., as Chromohalobacter marismortui comb. nov., nom. rev. *Int. J. Syst. Bacteriol.* **1989**, *39*, 382–386. [CrossRef]

33. Rivadeneyra, A.; Rivadeneyra, M.A.; Escamilla, C.V.; Algarra, A.M.; Navas, A.S.; Martín-Ramos, J.D. The influence of Salt Concentration on the Precipitation of Magnesium Calcite and Calcium Dolomite by Halomonas Anticariensis. *Expert Opin. Environ. Biol.* **2016**. [CrossRef]

34. Deng, S.C.; Dong, H.L.; Lv, G.; Jiang, H.C.; Yu, B.S.; Bishop, M.E. Microbial dolomite precipitation using sulfate reducing and halophilic bacteria: Results from Qinghai Lake, Tibetan Plateau, NW China. *Chem. Geol.* **2010**, *278*, 151–159. [CrossRef]

35. Babavalian, H.; Amoozegar, M.A.; Pourbabaee, A.A.; Moghaddam, M.M.; Shakeri, F. Isolation and identification of moderately halophilic bacteria producing hydrolytic enzymes from the largest hypersaline playa in Iran. *Microbiology* **2013**, *82*, 466–474. [CrossRef]

36. Kim, C.S.; Lee, C.H.; Shin, J.S.; Chung, Y.S.; Hyung, N.I. A simple and rapid method for isolation of high quality genomic DNA from fruit trees and conifers using PVP. *Nucleic Acids Res.* **1997**, *25*, 1085–1086. [CrossRef] [PubMed]

37. Madhaiyan, M.; Poonguzhali, S.; Kwon, S.W.; Sa, T.M. Methylobacterium *phyllosphaerae* sp. nov., a pink-pigmented, facultative methylotroph from rice. *Int. J. Syst. Evol. Microbiol.* **2009**, *59*, 22–27. [CrossRef] [PubMed]

38. Weisburg, W.G.; Barns, S.M.; Pelletier, D.A.; Lane, D.J. 16S ribosomal DNA amplification for phylogenetic study. *J. Bacteriol.* **1991**, *2*, 697–703. [CrossRef]

39. Smith, K.S.; Ferry, J.G. A plant-type (β-class) carbonic anhydrase in the thermophilic methanoarchaeon Methanobacterium thermoautotrophicum. *J. Bacteriol.* **1999**, *181*, 6247–6253. [PubMed]

40. Goldsmith, J.R.; Graf, D.L.; Heard, H.C. Lattice constants of the calcium-magnesium carbonates. *Am. Mineral.* **1961**, *46*, 453–457.

41. Arvidson, R.S.; Mackenzie, F.T. The dolomite problem: Control of precipitation kinetics by temperature and saturation state. *Am. J. Sci.* **1999**, *299*, 257–288. [CrossRef]

42. Guo, C.; Liu, H.Z.; Wang, J.; Chen, J.Y. Conformational structure of triblock copolymers by FT-Raman and FTIR spectroscopy. *J. Colloid Interface Sci.* **1999**, *209*, 368–373. [CrossRef] [PubMed]

43. Su, Y.L.; Liu, H.Z.; Guo, C.; Wang, J. Association behavior of PEO–PPO–PEO block copolymers in water or organic solvent observed by FTIR spectroscopy. *Mol. Simul.* **2003**, *29*, 803–808. [CrossRef]

44. Achal, V.; Pan, X.L. Characterization of urease and carbonic anhydrase producing bacteria and their role in calcite precipitation. *Curr. Microbiol.* **2011**, *62*, 894–902. [CrossRef] [PubMed]

45. Han, Z.Z.; Sun, B.; Zhao, H.; Yan, H.X.; Han, M.; Zhao, Y.Y.; Meng, R.R.; Zhuang, D.X.; Li, D.; Ma, Y.T.; et al. Isolation of *Leclercia adcarboxglata* Strain JLS1 from the dolostone sample and characterization of its induced struvite minerals. *Geomicrobiol. J.* **2017**, 1–11. [CrossRef]

46. De Muynck, W.; De Belie, N.; Verstraete, W. Microbial carbonate precipitation in construction materials: A review. *Ecol. Eng.* **2010**, *36*, 118–136. [CrossRef]

47. Han, Z.Z.; Zhuang, D.X.; Yan, H.X.; Zhao, H.; Sun, B.; Li, D.; Sun, Y.W.; Hu, W.Y.; Xuan, Q.Z.; Chen, J.A.; et al. Thermogravimetric and kinetic analysis of thermal decomposition characteristics of microbial calcites induced by cyanobacteria *Synechocystis* sp. PCC6803. *J. Therm. Anal. Calorim.* **2017**, *127*, 1371–1379. [CrossRef]

48. Wang, Y.Y.; Yao, Q.Z.; Zhou, G.T.; Fu, S.Q. Formation of elongated calcite mesocrystals and implication for biomineralization. *Chem. Geol.* **2013**, *360–361*, 126–133. [CrossRef]

49. Fukushi, K.; Munemoto, T.; Sakai, M.; Yagi, S. Monohydrocalcite: A promising remediation material for hazardous anions. *Sci. Technol. Adv. Mater.* **2011**, *12*, 1–12. [CrossRef] [PubMed]

50. Nishiyama, R.; Munemoto, T.; Fukushi, K. Formation condition of monohydrocalcite from $CaCl_2$-$MgCl_2$-Na_2CO_3 solutions. *Geochim. Cosmochim. Acta* **2013**, *100*, 217–231. [CrossRef]

51. Kimura, T.; Koga, N. Monohydrocalcite in comparisonwith hydrated amorphous calcium carbonate: Precipitation condition and thermal behavior. *Cryst. Growth Des.* **2011**, *11*, 3877–3884. [CrossRef]

52. Han, Z.Z.; Meng, R.R.; Yan, H.X.; Zhao, H.; Han, M.; Zhao, Y.Y.; Sun, B.; Sun, Y.B.; Wang, J.; Zhuang, D.X.; et al. Calcium carbonate precipitation by *Synechocystis* sp. PCC6803 at different Mg/Ca molar ratios under the laboratory condition. *Carbonate Evaporite* **2016**, 1–15. [CrossRef]

53. Porter, S.M. Seawater chemistry and early carbonates biomineralization. *Science* **2007**, *316*, 1302. [CrossRef] [PubMed]

54. Bontognali, T.R.R.; Vasconcelos, C.; Warthmann, R.J.; Dupraz, C.; Bernasconi, S.M.; McKenzie, J.A. Microbes produce nanobacteria-like structures, avoiding entombment. *Geology* **2008**, *36*, 663–666. [CrossRef]

55. Kenward, P.A.; Goldstein, R.H.; Gonzalez, L.A.; Roberts, J.A. Precipitation of low-temperature dolomite from an anaerobic microbial consortium: The role of methanogenic Archaea. *Geobiology* **2009**, *7*, 556–565. [CrossRef] [PubMed]

56. Li, Q.; Wang, Q.F.; Zhu, J.Y.; Zhou, S.; Gan, M.; Jiang, H.; Sand, W.G. Effect of Extracellular Polymeric Substances on Surface Properties and Attachment Behavior of *Acidithiobacillus ferrooxidans*. *Minerals* **2016**, *6*, 1–11. [CrossRef]

57. Han, Z.Z.; Yan, H.X.; Zhao, H.; Zhou, S.X.; Han, M.; Meng, X.Q.; Zhang, Y.; Zhao, Y.Y.; Sun, B.; Yao, C.K.; et al. Bio-precipitation of Calcite with Preferential Orientation Induced by *Synechocystis* sp. PCC6803. *Geomicrobiol. J.* **2014**, *31*, 884–899. [CrossRef]

58. Sheng, G.P.; Yu, H.Q.; Li, X.Y. Extracellular polymeric substances (EPS) of microbial aggregates in biological wastewater treatment systems: A review. *Biotechnol. Adv.* **2010**, *28*, 882–894. [CrossRef] [PubMed]

59. Jaisi, D.P.; Dong, H.L.; Kim, J.W.; He, Z.Q.; Morton, J.P. Nontronite particle aggregation induced by microbial Fe(III) reduction and exopolysaccharide production. *Clays Clay Miner.* **2007**, *55*, 96–107. [CrossRef]

60. Von Weymarn, N.; Nyyssölä, A.; Reinikainen, T.; Leisola, M.; Ojamo, H. Improved osmotolerance of recombinant Escherichia coli by de novo glycine betaine biosynthesis. *Appl. Microbiol. Biotechnol.* **2001**, *55*, 214–218. [CrossRef] [PubMed]